FUNCTIONALIZED METAL ORGANINC FRAMEWORK FOR CHEMOTHERAPY DRUG DELIVERY

by

Ahmed H.S Ahmed

A Thesis presented to the Faculty of the
American University of Sharjah
College of Engineering
In Partial Fulfillment
of the Requirements
for the Degree of

Master of Science in
Chemical Engineering

Sharjah, United Arab Emirates

November 2020

Declaration of Authorship

I declare that this thesis is my own work and, to the best of my knowledge and belief, it does not contain material published or written by a third party, except where permission has been obtained and/or appropriately cited through full and accurate referencing.

Signature ……AHMED …….

Date……..…17-Dec-20……..……

Approval Signatures

We, the undersigned, approve the Master's Thesis of Ahmed H.S Ahmed

Thesis Title: Functionalized Metal Organic Frameworks For Chemotherapy Drug Delivery

Date of Defense: 19/11/2020

Name, Title and Affiliation	**Signature**
Dr. Rana Sabouni Associate Professor, Department of Chemical Engineering Thesis Advisor	
Dr. Ghaleb Husseini Professor , Department of Chemical Engineering Thesis Co-Advisor	
Dr. Zarook Shareefdeen Professor, Department of Chemical Engineering Thesis Committee Member	
Dr. Nahid Awad Visiting Scholar Thesis Committee Member	
Dr. Sameer Al-Asheh Head, Department of Chemical Engineering	
Dr. Lotfi Romdhane Associate Dean for Graduate Affairs and Research College of Engineering	
Dr. Sirin Tekinay Dean College of Engineering	
Dr. Mohamed El-Tarhuni Vice Provost for Graduate Studies Office of Graduate Studies	

Acknowledgement

I would like to give my sincere gratitude and appreciation to my mentor and advisor Dr. Rana Sabouni, her continues support, dedication and generosity was the main reason I was able to finish my thesis work and master's program . Dr. Rana has been an excellent mentor to me and other colleagues and it was an honor working under her supervision. Her care and advice allowed me to grow on both professional and personal level.

I would to express my sincere appreciation to Dr. Ghaleb Husseini for his outstanding motivation and support. His advice and care allowed me and the rest of the drug delivery group to perform and produce notable work.

I would like to give my sincere gratitude to Eng, Nour Al-Sawafta, Eng. Abdollah Al Karami and Eng. Vinud Paul for their help and support in experimental work and data analysis.

I would like to expresses my appreciation to Dr. Nahid Awad as a committee member and as a supervisor in the drug delivery lab. Her advice, comments and support contributed in enhancing the quality of this work.

I would like to thank Dr. Zarook Sharafdeen for his comments and advice as a committee member. His comment and advice also raised the quality of this work.

I would like to express my deepest appreciation to Dr. Sameer AL-Asheh for his mentorship and support along my academic years. It's has been a huge honor being educated by and under his supervision.

Also I Would like to express my deepest gratitude to the American university of Sharjah and the Chemical Engineering Department, for giving me the opportunity to be enrolled in this master's program and granting me the GTA Assistantship.

Last but not least, I would like to express my deepest gratitude and appreciation to my family, friends and colleagues for their continues support along the way.

Dedication

To
Hosni Radwan
Aida Disi
Effat Disi
Adle Disi
Shorouq AL-Haj
Farah Ahmed
Leen Ahmed …

Abstract

Cancer is the leading cause of death worldwide, and can be treated by various methods or sometimes a combination of different treatments. Chemotherapy is one of the conventional methods of treatment. Although it is effective in killing cancer cells, it affects other fast-growing healthy cells, resulting in several significant health issues. Metal organic frameworks (MOFs) gained tremendous scientific attention for their extraordinary physical and chemical properties. The use of metal organic frameworks was investigated in many applications, and recently they have been used in biomedical applications such as drug delivery. This work aims to investigate an engineered PEG-folate-functionalized metal organic framework as anticancer nanocarriers, specifically targeting cancerous via the folate moiety and using ultrasound as an external stimulus. An iron-based MOF was synthesized under microwave irradiation using $FeCl_3$.6 (H_2O) and 2-Aminoterephthalic acid (NH_2-BDC) Furthermore, the synthesized MOF was surface modified to conjugate a folic acid group that allows for the active targeting of cancer cells. The synthesized MOF was characterized using Fourier-Transform Infrared Spectroscopy (FTIR), Thermogravimetric Analysis (TGA) and Dynamic Light Scattering (DLS). The encapsulation efficiencies and release profiles of the prepared MOF samples were studied using a model drug (namely calcein) and an anticancer drug (namely Doxorubicin, DOX) under different pH values (5, 6.4, and 7.4) with and without ultrasound. The encapsulation efficiency was determined to be in the range of 88-90% for calcein and 95-97% for DOX under pHs of 5, 6.4, and 7.4, respectively. Furthermore, low-frequency ultrasound (at 35 kHz) demonstrated the sono-sensitivity of PEG-folate-functionalized MOFs samples with release efficiencies of 44.4 % for DOX at 7.4 pH, 70.2% at 5.3 pH with PEG-FA modification, and 90% at 5.3 pH without PEG-FA modification within 280 mins compared to a control study (without ultrasound) of 14%, 14%, and 16%, respectively. Moreover, the release kinetics of both studies were studied and fitted to 9 different drug release models. Finally, statistical analysis confirms the significance of ultrasound triggered release. Accordingly, it is anticipated that using ultrasound as an external triggering mechanism with MOFs will help initiate a new generation of smart drug delivery systems in the fight against cancer.

Keywords: metal organic frameworks, drug delivery, ultrasound, triggered releases, release kinetics and encapsulation efficiency.

Table of Contents

List of Figures

List of Tables

Chapter 1. Introduction

1.1 Overview

Cancer has gained tremendous attention worldwide, as it became one of the major topics in modern medicine. Cancer comprises a large group of diseases, and many of its forms are lethal. Although there are many types of cancer, all cancer cells share one common characteristic in which their cell division mechanism is disrupted. As a result, cancer arises from abnormal cell growth or division. In many cases, these damaged cells will develop, spread, and divide, resulting in a tumor. The tumor may grow in size, and may spread to other regions in the body, a process known as metastasis.

1.1.1. Cancer treatment. Different cancer treatments are available, and each treatment depends on the type and the stage of cancer, which vary from a patient to another. Moreover, a patient may need to be treated with a combination of therapies, including surgery, radiation, chemotherapy, hormonal therapy, targeted therapy, and synthetic lethality. For example, a patient may need to undergo surgery to remove the solid tumor followed by chemotherapy or radiation therapy to eliminate any cancerous cells remaining traces.

Although surgery is the oldest form of cancer therapy and is an effective treatment for many types of cancer, yet it can be implemented mainly in the early stages of the disease, before the metastasis of cancer. Surgeons use several tools to surgically remove the tumor, such as scalpels, laser, hyperthermia, and photodynamic therapy. When using scalpels and sharp surgical instruments, surgeons physically cut through the body and excise the tumor. On the other hand, the surgical method includes other techniques such as cryosurgery in which the abnormal tissues or cells are treated/destroyed with extremely low temperatures using liquid nitrogen or argon gas [1].In addition, the laser surgical treatment, which includes a powerful beam of light cuts through the skin and destroy, reduce or inhibit the cancerous cells. The laser is used for precise surgeries, where high accuracy is needed [1].

Furthermore, hyperthermia is a technique in which a small region or the cancerous tissue is exposed to high temperatures. High temperature destroys the cancer cells and increases their susceptibility to radiation or chemotherapy [1]. Finally, another

technique used in the surgical treatment of cancers is photodynamic therapy (PDT). “Photodynamic therapy is a form of phototherapy that involves three key components: a photosensitizer, a light source, and tissue oxygen. When these components are combined, they become toxic to the targeted cells. The wavelength of the light source needs to be appropriate for exciting the photosensitizer to produce reactive oxygen species” [2].

Another common cancer treatment is radiation therapy or radiotherapy. Radiotherapy uses high doses of radiation to destroy and reduce the size of the tumor [3]. The radiation from the radiotherapy kills or inhibits tumor growth by damaging the DNA of the cancerous cells. A cell with damaged DNA will not be able to grow, divide and repair itself and eventually die. Radiotherapy can be delivered in two ways, internally or externally. For external radiotherapy, an external high-energy X-ray beam is directed into cancer. On the other hand, the internal radiation involves injecting the patient with a radioactive material that seeks out the cancerous cells and destroys them [3].

In addition, chemotherapy is another conventional cancer treatment method. The purpose of chemotherapy is to inhibit cell division and growth. The chemotherapeutic drugs mainly damage the DNA or RNA (genetic material) of the cell to suppress growth or eventually eradicate the cell itself. Since cell division or multiplication is a characteristic of both normal and cancerous cells, both cells are affected by the drug, especially those with a rapid rate turnover, such as bone marrow and mucous membranes [4]. Therefore, it is crucial to find a drug that is effective in controlling the growth and vitality of the cancerous cells, yet has a minimal effect on healthy cells. Moreover, chemotherapy is used in duel therapeutic methods such us being used alongside surgical procedures and radiation therapy to eradicate cancerous cells present in the patient’s body.

1.1.2. Drug carriers. Bioavailability is a major concern for drug therapy, as it is a key step in ensuring the bio-efficiency of the drugs. Bioavailability is the portion of the drug that enters the body and is still biologically active to accomplish its purpose. The bioavailability of pharmaceutical drugs is limited due to the drugs’ low water solubility. Since the human body has high water content, some of the drugs lose their effectiveness. Moreover, these drugs need to be lipophilic with a specific polarity to

cross or enter the lipophilic cell membrane. Drug delivery can tremendously overcome some of these limitations. Recent advancements in drug delivery systems have shown that drug carriers can be used as an effective method to protect, increase the bioavailability of the drug and prolong its presence in the blood [5]. Besides, the release of the encapsulated drug can be designed and controlled according to the type of material used to synthesize drug carriers. Several chemicals and organic materials have been investigated as drug carriers, including liposomes, polymeric micelles, and nanoparticles.

The approach of drug delivery by drug carriers can be divided into four steps. The first step is the loading or encapsulation of the drug into the nanovehicles. Next is the delivery of the drug to the specified organ or tissue, then the uptake of the drug-carrier complex by the cells, and finally the release of the drug from the carrier at the tumor site [5].

1.1.2.1 ***Liposomes.*** Liposomes are spherical vesicles consisting of one or more phospholipid bilayers. The spherical structure has an aqueous center in which hydrophilic drugs are encapsulated, while the hydrophobic and lipophilic drugs are encapsulated between the phospholipid bilayers [6]. Over the last 50 years, liposomes have gained considerable attention as promising drug carriers due to their exceptional properties. Liposomes protect the encapsulated drugs from early inactivation, degradation, and dilution in the circulation system [6] and provide a pathway to hydrophobic lipophilic drugs to the targeted tissue to increase the efficiency of the drug. Last but not least, the surface of the liposomes could be modified by conjugating functional groups and ligands to serve its purpose or enhance its efficacy. The accelerated blood clearance phenomenon adversely affects the performance of the liposomes as drug carriers [7]. To solve this problem, polyethylene glycol molecules are grafted on the surface of these liposomes in an attempt to reduce their recognition of the reticuloendothelial system (RES). To render these nanocarriers more target specific, ligands are attached to their surface. These ligands are able to bind to receptors on the surface of cancer cells and initiate receptor-mediated endocytosis. For example, folic acid is attached to the surface of the liposome as an active targeting ligand. Folic acid has a high affinity towards folate receptors, which are highly overexpressed on the surface of several cancers [7].

1.1.2.2 ***Polymeric micelles***. One of the major challenges in drug delivery systems is the removal of the nanocarriers by the blood circulation before reaching the specified tissue or organ. As mentioned previously, one of the most effective methods to prolong the availability of the drug in blood circulation is the surface coating of a hydrophilic polymer, e.g., polyethylene glycol (PEG) [7]. This coating provides protection to the drug carrier from identification and destruction by the immune system. Polymeric micelles are made up of a hydrophilic shell and a hydrophobic core. The hydrophobic drug is encapsulated in the hydrophobic core, while the hydrophilic shell provides protection and increases the bioavailability of the therapeutic agent [8]. The use of polymeric micelles in drug delivery reduces the cytotoxicity of the drug. It increases its concentration at the diseased site as it delivers it to the specified target minimizing its effect on healthy cells. Having an appropriate size, the polymeric micelles are easily forced out from the blood vessels by the enhanced permeability and retention effect and are allowed to accumulate at the tumor's site [8]. Similar to liposomes, micelles could be functionalized by conjugating targeting molecules on the surface of the micelle to enhance its performance. Also, probes and imaging agents are coupled with the micelle for tumor imaging and diagnoses.

1.1.2.3 ***Metal-Organic Frameworks (MOFs).*** Metal organic frameworks (MOFs) are porous hybrid materials that are typically formed by the self-assembly of inorganic nodes like metal ions or clusters and organic linkers as shown in Figure 1.

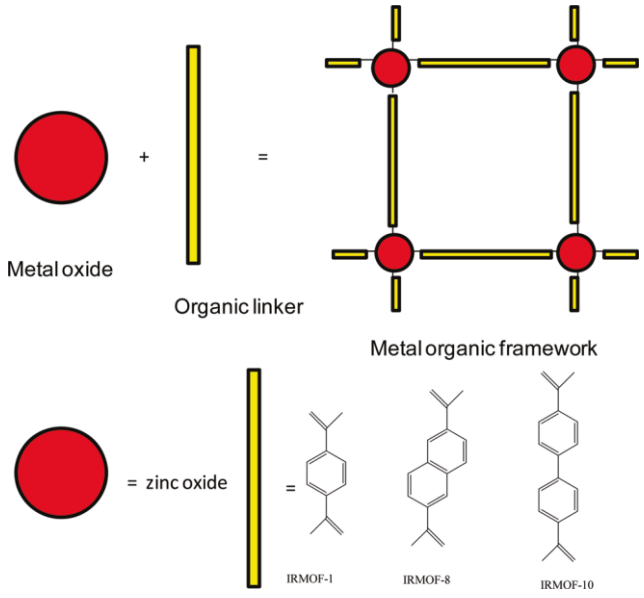

Figure 1: Building block of a metal organic framework [12].

Recently, nano-scaled MOFs have gained a tremendous interest in versatile industrial applications due to their extraordinary physical and chemical properties. MOFs have a huge surface area that exceeds 6000 m^2/g and high porosity that reaches up to 90% of its volume [9]. Moreover, an important characteristic of MOFs is the ease of structural tuning and surface modification, which aids the molecule in serving its purpose. MOFs have attracted much attention for applications in gas storage and separation, catalysis and biomedical applications, such as bio sensors and drug delivery (Figure 2).

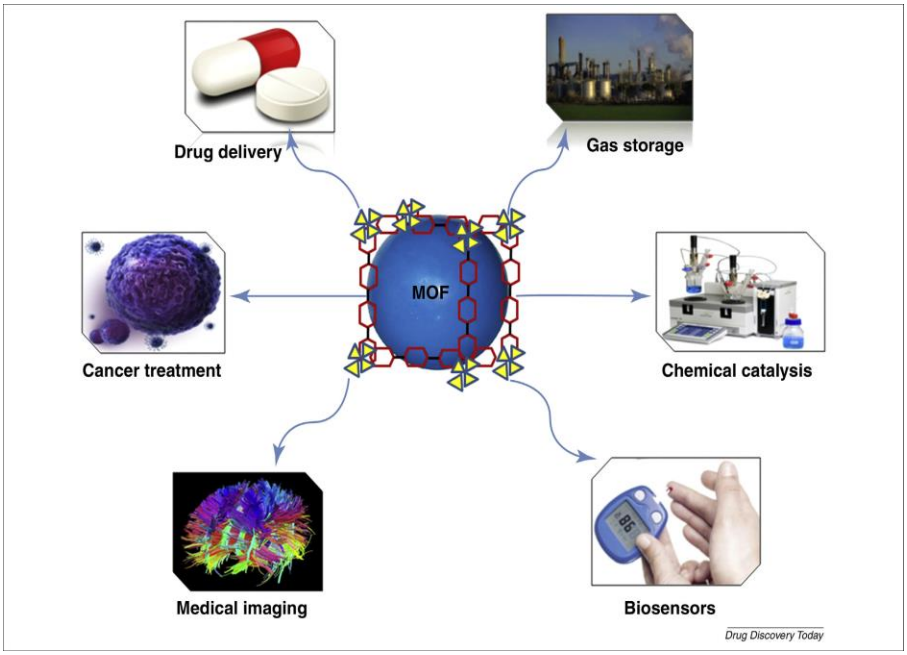

Figure 2: Industrial applications of metal organic frameworks[10].

1.2 Thesis Objective

The main aim of this thesis is to develop new smart drug carriers for delivering a model drug (namely calcein) and an anti-neoplastic agent (namely DOX) using PEG-folate functionalized MOFs and ultrasound as triggering stimulus. Accordingly, the objectives of this thesis are to:

1. Investigate the facile synthesis technique using microwave irradiation to synthesize MOFs in comparison to the conventional oven synthesis technique.
2. Synthesize and characterize functionalized metal organic frameworks (NH_2-Fe BDC MOFs) using amino-functionalized organic ligands as control MOFs.

3. Synthesize and characterize PEG-FA-MOFs targeted MOFs.
4. Investigate the loading and release efficiencies of the model drug calcein and the anticancer drug DOX.
5. Study the effect of ultrasound on the drug release kinetics at different pH values (5.0, 6.4 and 7.4).
6. Model drug release kinetics by fitting experimental release data to several kinetic models.

1.3 Thesis Organization

The Thesis is organized as the following:

- Chapter 2: Literature Review
- Chapter 3: Materials and Methods
- Chapter 4: Results and Discussion
- Chapter 5: Conclusion and Future work

Chapter 2. Literature Review

2.1 Background Information

The scientific investigation of the MOFs started in the 1990s [10]. This area's scope in chemistry is very wide due to the vast number of possible metal-organic combinations. As mentioned previously, metal organic frameworks have several considerable attractive properties, including diverse topology, pore size tunability, high surface area, high porosity, surface functionality, and excellent biocompatibility. These characteristics allow MOFs to be used as efficient drug delivery carriers by encapsulating therapeutic drugs inside their structures or by adsorbing the agent on their surface. In addition, unlike other nanocarriers that release the drug in bursts (a challenge in drug delivery), the MOFs release mechanism is slow and controlled by matrix degradation, which improves the effectiveness of the treatment [10]. Furthermore, using MOFs as drug carriers increases the treatment's efficiency by increasing the drug bioavailability and actively targeting the specified tissues through surface functionality.

2.1.1. MOF structure. The building blocks of metal organic frameworks consist of metal ions and organic linkers. According to Rowswell et al. [11], there are three attributes to classify the solid or the composite to be a MOF: a strong bonding (robustness), linking units, and a well geometrical crystal structure. Depending on the synthetic stages, MOFs are classified as first-generation (normal), second-generation (functionalized), and third-generation (smart). First-generation MOFs are of the normal structure with a metal-ion linked to an organic ligand. The second-generation MOFs include a modified surface to serve a specific purpose. The third-generation MOFs contains encapsulated drugs or bioactive material in their framework [12].

Additionally, MOFs could be classified according to the robustness of the structure. MOFs are classified as rigid or flexible MOFs. Flexible MOFs have the ability to reversibly change their structure in the presence of stimuli, such as encapsulated material, temperature, and pressure [13].

Horcajdha et al. have successfully encapsulated several therapeutic agents into MOFs, including Ibuprofen. They studied MIL-53-Cr, MIL-53-Fe, and MIL-100 as drug carriers. Rigid MOFS, such as the MIL-100, showed a high drug loading capacity

with 1.4 g of drug per gram of MOF and a controlled drug release for up to six days [13].

In addition, the same research group investigated the breathing effect of flexible structures such as the MIL-53 family. The breathing effect allows the structure to modulate the pore size, depending on the encapsulated drug (Figure 3). This effect may increase the void volume of the MOF from 50% to 230%. The MIL-53 adsorbed around 20% wt. of the drug and had a controlled release of 3 weeks with zero-order kinetics [13].

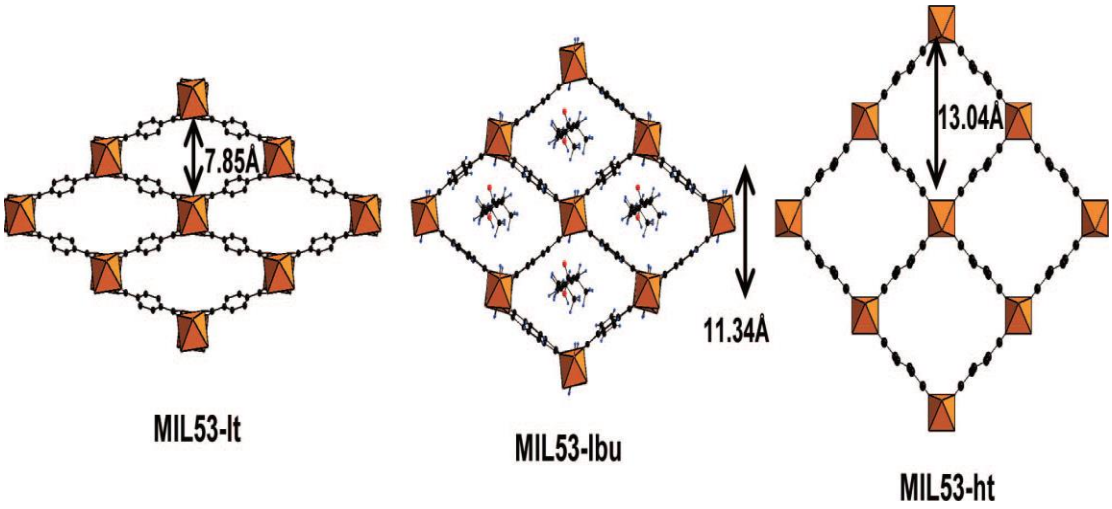

Figure 3: Breathing effect in flexible MOFs[13].

Furthermore, classifying MOFs based on their crystal structure arrangements, MOFs can be sorted as crystalline or amorphous [14]. Crystalline MOFs possess an infinite arrangement of regular solid porous framework alongside a long-range order. The amorphous structure follows the opposite trend and tends to be more flexible [13].

2.1.2. Surface modification. The surface of the MOFs could be modified to enhance its performance. Mainly a ligand will be conjugated to the active sites of the MOF's surface. These ligands could be functional groups, i.e., polymer or biomolecules. These surface modifications enhance water dispersibility, stability, improve drug loading, and reduce protein binding alongside adding targeting groups to enhance drug delivery (Figure 5)[15].

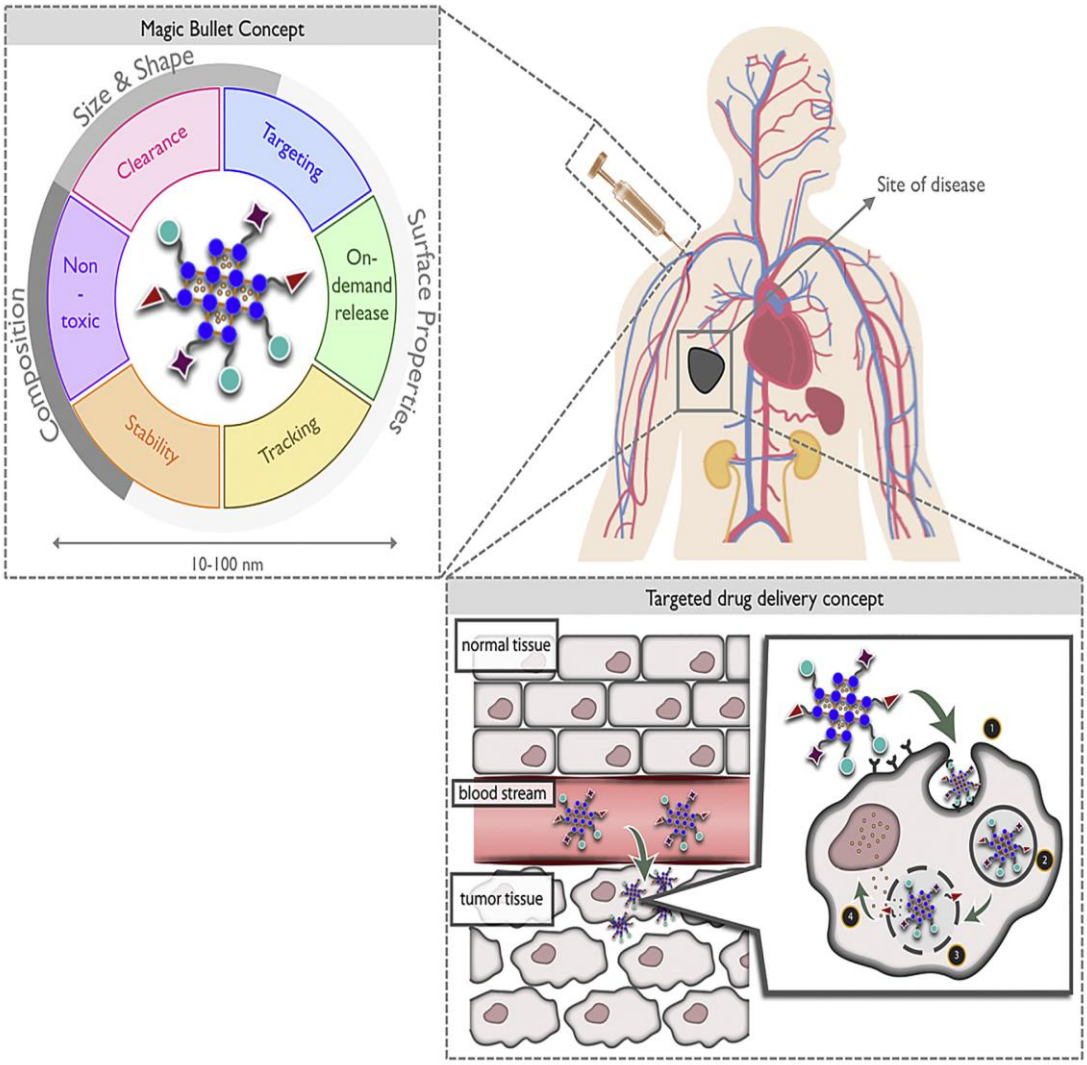

Figure 4: The general concepts of using MOFs as a drug delivery system [19].

Numerous modification techniques are implemented to modify the surface of the MOF. The first method is polymer-functionalizing; this technique overlays a silica or polymer coating on the surface of the MOF (Figure 4). The silica coating improves biocompatibility and enhances water dispersibility and provides further MOF surface modification [16]. Likewise, polymer coating offers similar enhancements to the MOF and provides more controlled drug release. Some studies showed that a combined silica and polymer surface modifications improve water solubility and dispersibility [10]. Furthermore, Mocniak et al. demonstrated a higher drug encapsulating efficiency for cisplatin and superior tumor targeting potential when a MIL-101 MOF is coated with silica [17].

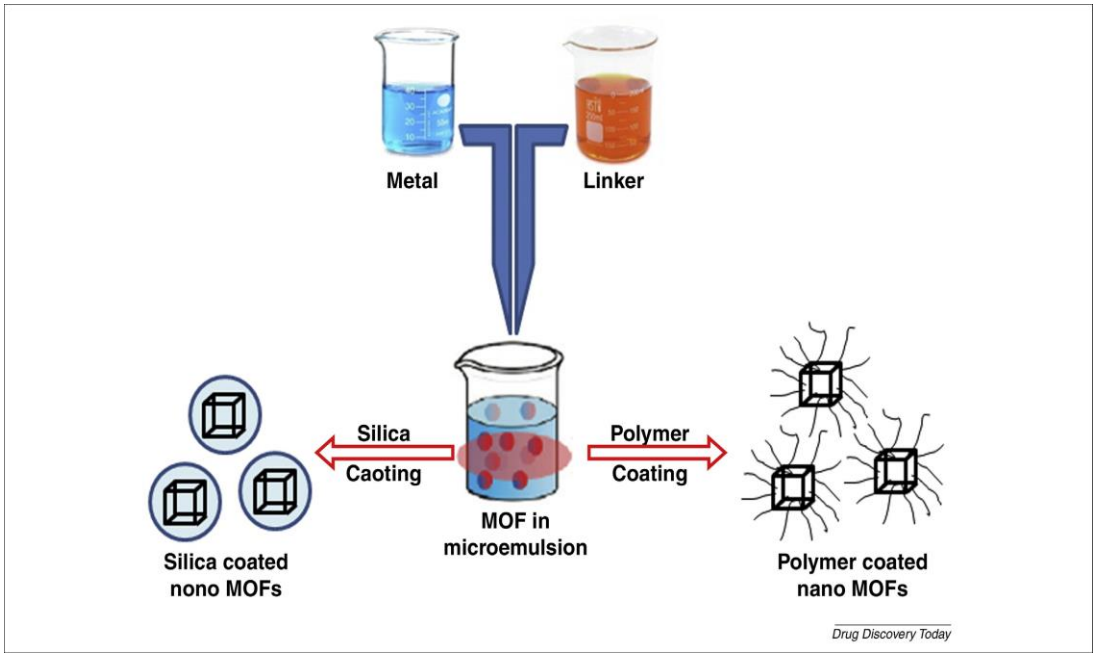

Figure 5:Silica and polymer coating in MOFs [10].

An alternative surface modification technique is PEG-functionalization. This technique aids the application of MOFs in the biomedical field and drug delivery. PEG-functionalization enhances water solubility and tumor targeting. Affinity molecules or ligands are attached to the active sites on the surface of the MOF. Such modification allows the MOFs to target the cancer cells and reduce the side effects of the drug on healthy cells. Furthermore, some of these ligands aid in diagnostic imaging in tumor treatment [10].

Last but not least, peptide-functionalization on the MOFs surfaces allows the attachment of fluorescent molecules for *in vitro* and *in vivo* diagnostic imaging alongside tumor targeting. This technique was investigated by McGuire and Forgan, where Rhodamine B moieties and targeting RGDfK peptides were grafted to a silica-coated MOF, for *in vitro* imaging and tumor targeting [18].

2.2 Synthesis Techniques of MOFs

Various approaches have been investigated lately to prepare metal organic frameworks depending on the reaction that links the metal ions to the organic linkers, including conventional solvothermal/hydrothermal technique and facile, rapid techniques (i.e., microwave, sonochemical, electrochemical and mechanochemical synthesis). Securing the desired extraordinary physical and chemical characteristics and

appropriate robustness of MOFs in a short reaction time can be challenging. Since the interactions between the metal clusters and organic linkers are weak, the reaction should be performed under certain conditions (Figure 6).

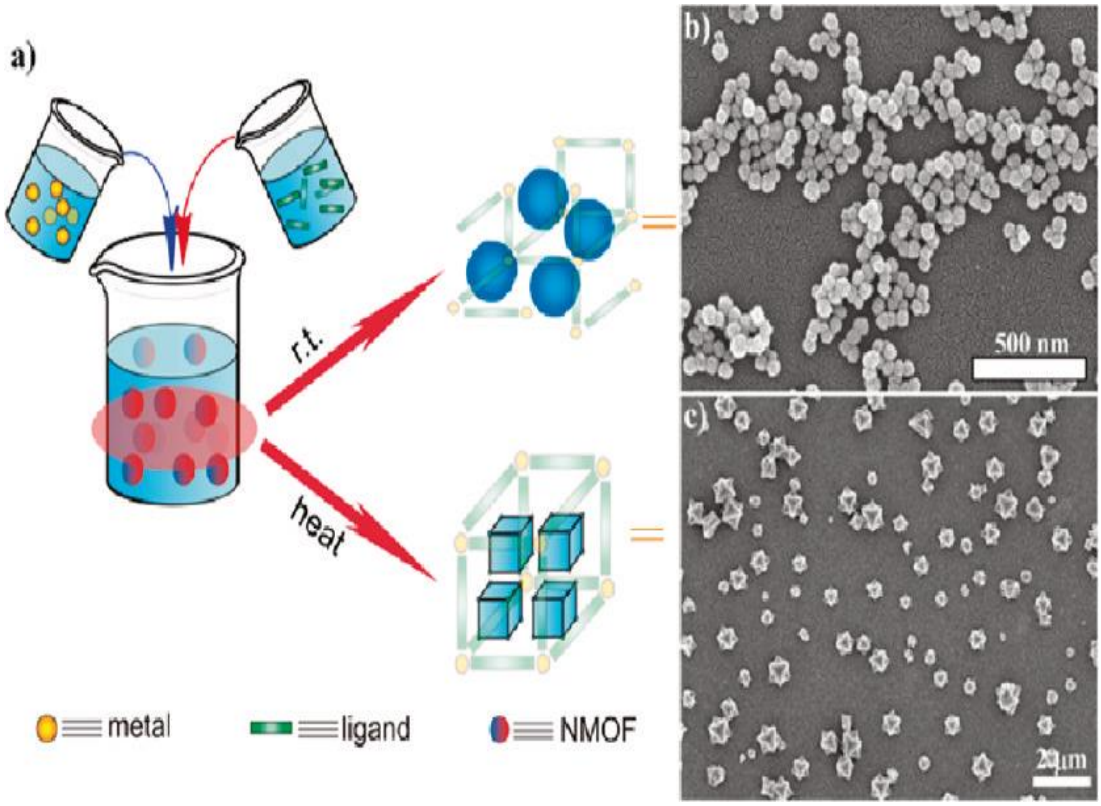

Figure 6: Difference between room temperature heating and assisted heating in terms of dimensions [16].

Many factors affect MOF's synthesis, including temperature, pressure, molar ratio, pH, and reaction time. The main parameter in this reaction is temperature. At higher temperatures, the produced MOFs will have a better crystalline structure and a proper morphology for their function. But the solvothermal reaction may have a long reaction time. Having a long reaction time may lead to product degradation or resulting in amorphous structure which affects the chemical loading or adsorbing properties of the metal organics frame work [20]. Therefore alternative synthesis routes are used to provide proper reaction conditions such as high temperature and high pressure in order to obtain the desired crystalline porous structure, as discussed in the following sections (Figure 7).

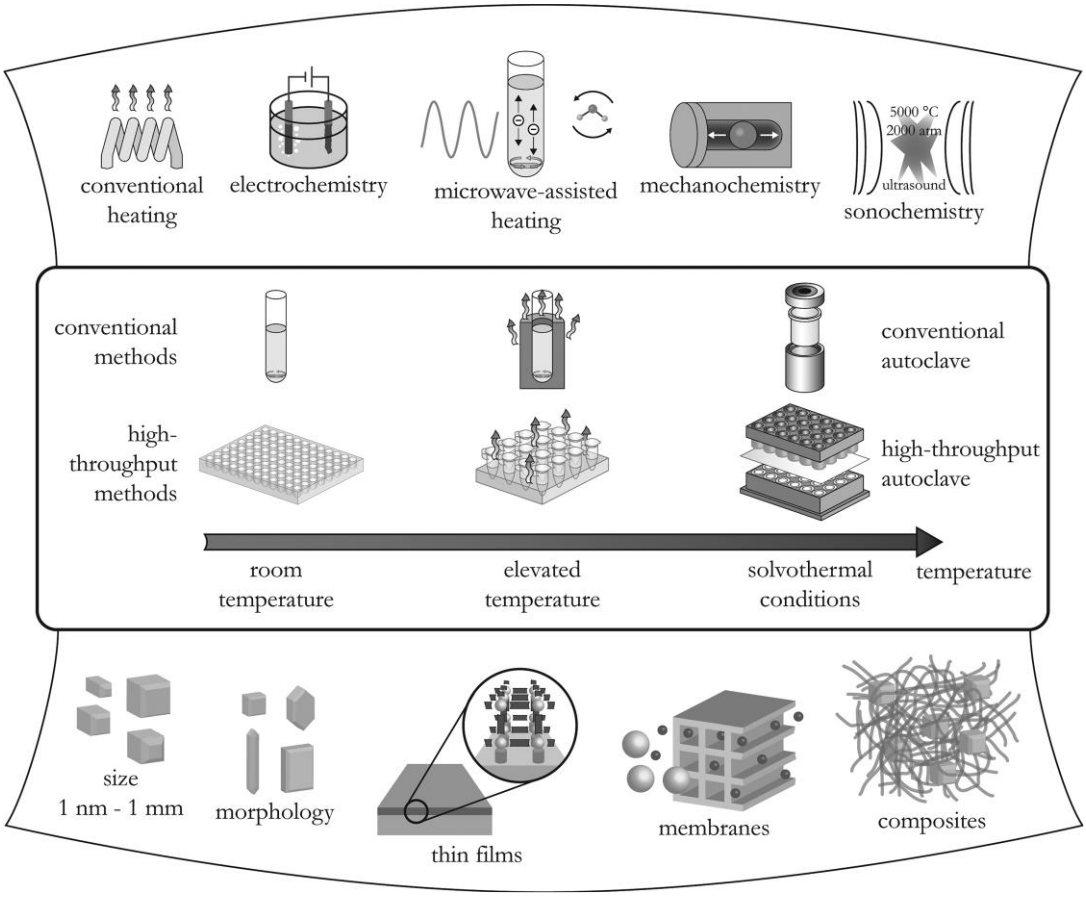

Figure 7: A general overview of different MOF synthesis methods [21].

2.2.1. Microwave assisted synthesis. Since the synthesis of metal organic frameworks requires a heating step for a long period of time, microwave-assisted heating has shown considerable benefits in reducing the reaction time by promoting a faster reaction rate in solution and solid-solid reactions. In solution reactions, electromagnetic waves interact with the free ions of the solution creating an oscillating magnetic field where the molecules permanently change their orientation. In solid–solid reactions, the electromagnetic waves conduct an electric current through the solid particles. As a result, heat will be produced to initiate the reaction. In microwave synthesis, few parameters must be considered, yet the temperature is the most crucial parameter in MOF synthesis [20]. The temperature is manipulated by changing the power output of the microwave. One of the main advantages of microwave heating is the homogeneous heat distribution throughout the sample. In addition, reaction time is also an important parameter to be considered. The microwave provides a higher temperature and pressure, which results in a higher reaction rate compared with the

conventional electric heating; therefore, allows faster synthesis of smaller crystals [20]. Other than providing a suitable heat distribution and shorter reaction time, the microwave-assisted synthesis is an efficient way to produce high purity nano-scaled MOFs with high mono-dispersity [22].

Vakili et al. applied the microwave-assisted synthesis to synthesize a Zn-based MOF (UiO-67). Compared with the conventional synthesis (the solvo-thermal technique), the microwave synthesis took only 2-2.5 hours, which is shorter than the case of solvo-thermal synthesis (~24 hours). Both reactions are conducted at the same temperature. Moreover, the microwave-assisted technique resulted in a higher yield and better porous properties [23]

2.2.2. Electrochemical synthesis. In electrochemical synthesis, the metal ions are introduced by anodic dissolution instead of metallic salts. In an electrochemical cell, the dissolved anodic metal interacts with the organic linker in the electrolyte. The main purpose of using this technique is to remove the use of anions, such as nitrate, perchlorate, or chloride during the synthesis, which is a challenge to scale-up [20]. Some metals might be reduced at the cathode; therefore, compounds such as acrylonitrile, acrylic, or maleic esters are used because they are favorably reduced more than most of the metals used in synthesizing MOFs [20]. The advantages of this technique include the higher solid content than the other methods and the ability to run the synthesis as a continuous process [20].

2.2.3. Mechanochemical synthesis. In this synthesis technique, mechanical force in the form of milling or grinding is used to initiate or conduct the reaction. The bond breakage and formation is done by physically applying a force on the reactants. This force will break the intermolecular forces between the reactants, change their orientations, and provide the required energy to form new bonds [24]. Recently, the rediscovery of mechanochemical synthesis in the pharmaceutical industry has attracted immense interest as a green synthesis technique allowing the use of solvent-free conditions [25].

Singh et al. successfully synthesized both singular and mixed rare earth metallic based MOFs. The scientists used Gd, Tn, and Dy as the metallic ions, in addition to

benzene 1, 3, 5-triboxylic acid as the organic linker. The MOFs were synthesized using mechanical milling in the absence of solvent [26].

In addition, Chen et al. applied the mechanochemical technique combined with the use of a liquid solvent to synthesize a water-stable indium-based MOF (InOF-1). The results showed that grinding for 20 minutes with CH_3CN (0.4 ml) lead to a high crystalline and porous product. The InOF-1 retained its crystal and porous structure in water for 12 hours [27].

2.2.4. Sonochemical synthesis. Sonochemistry involves the application of high energy ultrasound to chemical reactions. Although ultrasound waves have frequencies higher than 20 kHz, yet they do not initiate a reaction as their wavelength is much greater than the molecular bonds. In liquids, the ultrasound waves create areas of high pressure called compressions and areas of low pressures called refractions. In the low-pressure area, specifically in the region where the pressure is under the vapor pressure, bubbles will be produced. The cavities grow in size due to pressure changes along with the diffusion of the solute vapor into its volume. The cavities keep growing in size along with the accumulated ultrasonic energy until they reach their maximum volume and eventually burst. The oscillation of the bubbles is referred to as cavitation. The cavitation process causes a rapid release of energy with extremely high temperatures and pressures in a very short period of time. Moreover, high shear stresses are noticed in the surrounding area [28]. Having high energy imparted on the surface of the solid causes cavitation to activate its surface. Once these extreme conditions activate the surface, bond breaking and bond formation are able to occur, initiating the reaction [29].

Bigdeli et al. synthesized a Zinc based MOF using the sonochemical technique. The study compared the sonochemical method with the conventional method. The characterization tests were similar in both methods. The study also showed that increasing the initial concentration of the reagent increases the particle size. Also, shorter reaction times lead (different powers of the ultrasonic irradiations) to smaller nanostructures [30].

In another study, Gharib et al. successfully synthesized TMU-23 MOF under room temperature and atmospheric pressure using ultrasonic irradiation. This method

enhanced the control of both particle size and morphology of the MOF. Moreover, it was realized that increasing the reaction time and initial concentration of the reagent increases the particle size [31].

2.3 Drug Delivery

Anticancer therapeutic agents have a number of barriers and challenges, including bioavailability, water dispersibility, solubility, along with drug biodistribution. The lack of selectivity, tumor-targeting ability, and clearance of drugs have been identified as key obstacles in the development of anticancer drugs [5]. Accordingly, numerous anticancer nanocarriers have been developed, including liposomes, micelles, nanoparticles, and metal organic frameworks. Metal organic frameworks (MOFs) are considered one of the most promising nanocarriers due to their high porosity, surface area, and tunable pore size and surface functionality. Furthermore, MOFs can be tuned toward nanoscale carriers (e.g., 20-300 nm) for suitable in-vivo applications [32]. These physical and chemical properties allow the MOFs to have a high loading capacity, increase the bioavailability of the drug, and have a wide range of hydrophilic and hydrophobic drugs that could be encapsulated in their voids. Moreover, the MOFs are able to sustain the release of the agent for days, since burst action release decreases the efficiency of the drug and the treatment. As mentioned earlier, the structure of the MOF could be modified to enhance its performance, e.g., surface coating, to increase water dispersibility and enhance its robustness. By conjugating functional groups to the surface of the MOF, PEG and peptides allow the carrier to target specific tissues, in addition to diagnostic imaging.

The toxicity of the MOF must be evaluated to ensure that there is no threat to the host. Therefore, cytotoxicity assays are performed to assess the hazards of the synthesized MOFs. Molecular size is a major parameter in cytotoxic analysis since it determines its biodistribution, translocation, cellular uptake, and excretion. Thus, using nanoparticles in drug delivery has advantages that include a small size with a higher surface area to volume ratio, which is easily absorbed by the cell tissue and easily distributed. Furthermore, the toxicity of metal organic frameworks arises due to the presence of metallic molecules. These metals accumulate in the body, each possessing a different degradation rate [33]. During synthesis, it is advisable to use metals with higher permissible limits of daily requirements such as iron, magnesium, calcium, and

zinc [10]. Metals such as chromium should be avoided since they accumulate in the body and have a very low human permissibility limit.

In literature, many researchers evaluated the cytotoxicity of MOFs. It is shown that they are suitable for *in vitro* and *in vivo* administration. Ruiz-Molina et al. studied the cytotoxicity of Zn (1, 4-bis (imidazol-1- ylmethyl) benzene) (Zn (bix)) on human promyelocytic leukemia HL-60 cells. After treatment, the cell viability was measured at 80% [34]. In addition, Ma et al. synthesized a Zinc based MOF as a drug carrier for 5-fluorouracil (5-FU). A cytotoxic assay was performed on HeLa and HEK293 cell lines. The MOFs were harmless against both cell lines. The cell viability was measured to be 80% and 50% maximal inhibitory concentration of 5 μg/ml [35]. Furthermore, Vasconcelos et al. studied the cytotoxicity of doxorubicin (DOX) loaded ZIF-8 MOFs. Nano-ZIF-8's cytotoxicity was analyzed over three different cell lines, namely mucoepidermoid carcinoma of the lung, colorectal adenocarcinoma, and promyelocytic leukemia. The analysis showed that the ZIF-8 did not show any toxic behavior even at high concentrations [36]. Moreover, Baati et al. conducted an *in vivo* cytotoxicity analysis with three different iron carboxylate MOFs. The MOFs were administrated to rats at high dosages and showed low toxicity. The MOFs were rapidly sequestered by the liver and spleen and then further biodegraded [37].

In addition to stability, the MOF's biocompatibility and biodegradability are vital parameters in drug delivery. Since the MOF's are administrated *in vivo* and *in vitro*, their biodegradability profiles must be considered since they might accumulate inside the body. Several *in vivo* and *in vitro* studies showed positive results when considering the biodegradability of some iron carboxylate MOFs such as MIL-88A, MIL-88b-4CH_3, and MIL 100 [38]. Moreover, the biocompatibility of MOFs is categorized based on the organic linkers. The stability of the MOFs must also be evaluated to prevent the hydrolytic cleavage of the covalent bonds between the organic linker and metal ions. The stability of the MOFs could be evaluated by performing tests to ensure no defect in their morphology [10].

2.4 Cancer Treatment

The application of MOFs in Cancer Treatment would be of great benefit. MOFs could reduce the side effect of chemotherapy, enhance the targeting of the drug, and provide imaging diagnostics of the tumor. Many studies in the literature have

successfully encapsulated anti-cancer therapeutic drugs and have provided suitable results in *in vivo* and *in vitro* tumor reduction. Taylor et al. studied the use of nanorods of $Mn(BDC)(H_2O)_2$ and nanoparticles of $MN_3(BTC)_2(H_2O)_6$ coated with Silica for the delivery of RGDFK peptide and rhodamine B dye. The study showed the antiangiogenic properties on HT-29 cells by the up-regulation of the Rvβ3 gene [39]. Zhuang et al. developed a ZIF-8 MOF to encapsulate camptothecin (CPT) and fluorescein. To evaluate the effectiveness of the treatment, the MOF was administrated to MCF-7 breast cancer cells. The study compared the CPT MOF treatment with free CPT treatment. The results showed that after 24 hours, the CPT MOF has a higher cell death than the free CPT treatment, which required 48 hours to exhibit toxic results [40]. He et al. studied the application of MOFs in ovarian cancer. They synthesized MOF encapsulated cisplatin and pooled siRNAs. The siRNAs are used to silence multiple drug resistance genes and reduce the resistance of ovarian cancer cells to cisplatin treatment. The administration of the loaded MOF showed an improvement in the chemotherapeutic treatment compared with the conventional treatment. This shows the efficiency of the MOFs in encapsulating multiple drugs for cancer treatment [41]. Maspoch et al. encapsulated several anti-cancer therapeutic drugs inside [Zn(II)-1,4-Bis(imidazole-1- yl) benzen] MOF. The chemotherapeutic drug DOX was encapsulated in the MOF; then, the treatment was compared with the conventional DOX treatment. The MOF treatment showed better cytotoxicity and better drug release compared to conventional treatment [42]. Rowe et al. synthesized a modified Gd-based MOFs. The MOFs encapsulated the therapeutic drug methotrexate. To evaluate the effectiveness of the treatment, studies were performed on FITZ-HSA tumor cells. The study resulted in significant cell growth inhibition by increasing cellular apoptosis [43]. Liu et al. integrated both chemo and photodynamic therapy with MOFs. The scientists synthesized MIL-100 MOFs, then fictionalized them by adding a photosynthesizer peptide along with a folate functional group for tumor targeting. The study resulted in enhanced treatment efficiency. The multi-functionalized MOF resulted in a significant *in vivo* tumor volume reduction over 14 days [44].

2.5 MOF Release Mechanism

Several drug release mechanisms have been implemented in MOF drug delivery. The release mechanisms are classified into two classes, intrinsic and extrinsic [45].

In the intrinsic class, stimuli such as pH, free diffusion, and molecular degradation are examined. In pH-controlled release, a neutral pH gradient between the environment and tumor tissue will offer a proper stimulus for the drug release [46]. Reza et al. prepared Zn-based MOF using the sonochemical method. The MOF was loaded with the chemotherapeutic drug DOX. The scientists studied the release profile at different pH values. Since the release is almost inactive at physiological pH conditions of pH=7.4, the MOF releases the drug only when it interacts with the cancerous environment, which is slightly acidic. Reza et al. compared the drug release at three different pHs; 7.4, 6.0, and 4.5. The results of the experiment showed that the highest drug release occurred at a pH of 4.5, which is about 98% of the encapsulated drug. At pH values of 6.0 and 7.4, the drug release percentages were 54% and 83%, respectively [47].

In another study, Sun et al. investigated the effect of pH on the release of 5-FU encapsulated into ZIF-8. The release efficiency reached up to 70% over a period of 72 hours [48]. Furthermore, Yan et al. studied the pH release profile of a modified ZIF-8 MOF loaded with DOX. The study results showed that at a pH value of 5.0 the MOF released over 60% of the drug, while in the case of a pH value 7.4, the MOF released less than 30% [49].

In the case of extrinsic stimuli, the triggering mechanism is achieved by one of these stimuli: temperature, biomimetic, infrared radiation, visible light, and ultrasound. In a study by Adhikari et al., the effect of biomimetic systems on drug releases from DOX loaded ZIF-7, and ZIF-8 MOFs was investigated. Experiments showed that the ZIF-7 stayed intact under acidic conditions until when the MOF came in contact with liposomes and micelles, the results confirmed successful release. The experiment resulted in a 3-hour controlled release of the agent from the ZIF-8 and a 10-hour controlled release from the ZIF-7 MOFs [50].

Furthermore, a study by Jia et al. demonstrated the use of MOFs in photodynamic therapy. A modified Au-based MOF was functionalized by a two-photon-absorbing (TPA) ligand. Furthermore, the MOFs samples were functionalized by assembling the photosensitizer methylene blue. The modified drug delivery system allows imaging diagnostic, tumor targeting, and photodynamic therapy. The photodynamic abilities of the MOFs are activated or triggered by near infra-red

radiation of wavelengths in the range of 700 to 1000 nm. In this study, the photodynamic therapy was triggered by a light with a wavelength of 808 nm [52]. Moreover, DNA-MOF plays a significant role in immunotherapy. A study by Wang et al. developed novel DNA functionalized MOFs (isMOFs) as a highly generic approach for the intracellular delivery of therapeutic nucleic acids. Cytosine−Phosphate−Guanosine (CPG) was attached to the MOF's surface by intrinsic coordination; moreover, the MOF was covered with calcium phosphate exoskeleton. The experimental procedure showed that the CPG is released in an environment where free phosphate ions are present, although the exoskeleton must be removed or dissociate in an acidic environment. Thus, without an acidic environment, the CPG was not released from the surface of the MOF [53].

Temperature changes could act as stimuli in triggering drug release from loaded MOFs. A study by Lin et al. demonstrated the effect of temperature on the release profile. A Zn-based MOF was loaded with the anticancer drug methotrexate. The experiment compared the release by changing two parameters; pH and temperature. Two pH values were considered, namely 7.4 and 6.5, alongside two different temperatures, 37 ^{o}C, and 42 ^{o}C. The experimental results showed that at higher temperatures, drug release percentages were higher [54]. According to literature, the drug release efficiency of MOFs samples can be improved using external stimuli. Therefore, the stimulus of choice in this work is the ultrasound.

2.6 PEG Functionalization

The main challenge in cancer treatment is minimizing the side effects of chemotherapeutic drugs on healthy normal tissues. The MOF’s ability to be surface modified enhances the targetability of the drug delivery system, thus administrating the drug to cancerous tissue preferentially. Glycosyl-phosphatidylinositol is a folate receptor that is overly expressed in a variety of cancer cells, including tumors of the lung, ovaries, and breast, and has a limited expression in healthy cells [56]. Folic acid is stable over a wide range of temperatures and pH values, is non-immunogenic, and binds with the folate receptor [57]. Functionalizing the surface of the MOF with a folic acid PEG allows the drug delivery to detect and target the cancer tissue or tumor, as shown in Figure 10.

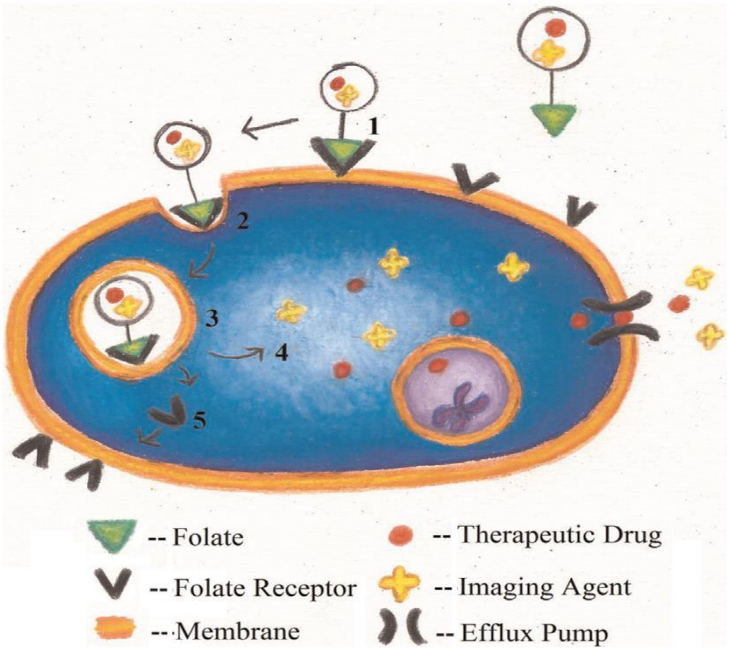

Figure 8: Folic acid-folate receptor interactions in drug delivery [58].

Tabasi et al. studied the cytotoxicity of folate-targeted mesoporous silicon DOX drug conjugates. The results of the experiment showed that mesoporous drug conjugates showed a higher cell death rate in cancer cells than free DOX [59]. In addition, a novel study was conducted by Thomas et al. to conjugate the chemotherapeutic drug methotrexate (MTX) on a dendrimer along with folic acid. The results of the experiment showed that the conjugate is 4300-fold higher affinity than free MTX. Thus, the polyvalent MTX on the dendrimer serves the dual role of a targeting molecule as well as a chemotherapeutic drug [60].

In this thesis, I combined the benefits of MOFs, folic acid, and ultrasound to research a novel drug delivery modality capable of sequestering two agents (a model drug, calcein, and an anti-neoplastic drug, DOX). Acoustic waves are then applied to release the contents of these carriers upon demand.

Chapter 3. Materials and Methods

3.1 Characterization

3.1.1. X-Ray diffraction analysis (XRD). X-Ray Diffraction or XRD is an analytical technique used to identify the morphology of a crystal structure, giving an indication of the unit dimensions. The apparatus of an XRD consists of three major parts; the X-ray tube, the sample holder, and the X-ray detector. A heating filament in the cathode ray tube generates the X-rays by producing electrons. The electrons strike the sample material [61]. Upon impact, the X-ray will scatter and separate in a distinct pattern called a diffraction pattern. Following Bragg's diffraction law, the diffraction pattern will provide an insight into the morphology of the crystal structure [62].

3.1.2. Thermogravimetric analysis (TGA). Thermogravimetric Analysis or TGA is a technique for measuring mass changes of a substance as a function of temperature. These changes could be a sign or an indication of processes including decomposition, degradation, sublimation, vaporization, adsorption, desorption, oxidation, and reduction [63]. TGA gives an indication of the thermal stability of the sample. The heating of the sample starts from100 ^{o}C up to 900 ^{o}C [64]. The TGA analysis was conducted using Perkin Elmer TGA instrument at a temperature ramp rate of 15 ^{o}C min^{-1}.

3.1.3. Fourier-transform infrared spectroscopy (FTIR). Fourier-transform infrared spectroscopy (FTIR) implements infrared radiation. When the infrared radiation passes through a sample; some of the radiation is absorbed while some is transmitted beyond the sample. Each chemical molecule has its own spectral fingerprint. The transmitted radiation sensed by the radiation detector of the apparatus identifies chemical molecules by interpreting its spectral fingerprint [65]. The FTIR characterization test was done with Spectrum one FTIR spectrometer by PerkinElmer within a wavelength range of 500 to 4000 cm^{-1}.

3.1.4. Scanning electron microscope (SEM). The scanning electron microscope uses focused high energy electrons on a solid surface generating a variety of signals to produce a high quality magnified image of the surface. This type of imaging provides information on the sample's morphology, chemical composition and crystallinity [66].

3.1.5. Dynamic light scattering (DLS). Dynamic light scattering (DLS) analysis measures and interprets light scattering data on a microsecond scale from the suspension of solids in a solution. This technique is used to determine particle size and dimensions. Usually, this analysis is used for dimensional identification of micron and nano-particles. Moreover, DLS can also be used as a probe of complex fluids, such as concentrated solutions [67]. The DLS characterization test was conducted through Dynapro Nanostar dynamic light scattering unit by WYATT Technology(USA).

3.1.6. UV-Visible spectrophotometer. UV-vis spectroscopy is based on the interaction between light and a chemical compound. As the light is absorbed by the compound, it results in the excitation of molecules and atoms to a higher energy state. The absorption of the light radiation releases a distinct spectrum for each compound. Therefore UV-VIS spectroscopy became an important tool in analytics and chemical identification [68].

3.2 Chemicals

All the chemicals and reagents used in the synthesis of functionalized MOFs were purchased from Sigma-Aldrich (supplied through LABCO LLC. Dubai, UAE). They are used without further modifications, including $FeCl_3.6(H_2O)$, 2-Aminoterephthalic acid (NH_2-BDC) and Dimethylformamide (DMF), which are used in the synthesis of the MOF. Furthermore, HOOC-poly-ethylene glycol (PEG-FA), 1-ethyl-3-(3-(dimethylamino)propyl)carbodiimide hydrochloride (EDC), and N-hydroxysuccinimide (NHS) are used in the surface modification and PEG functionalization of the MOF. Calcein is used as a model drug/dye, DOX as the chemotherapeutic drug.

3.3 Synthesis of NH_2-Fe BDC MOFs

The synthesis of MOF implemented the microwave irradiation technique. After synthesis, the MOF was modified in order to conjugate the folic acid group on the nanocarriers for active targeting. Calcein has fluorescent properties; thus, the loading and release efficiencies were measured using a spectrofluorometer (QuantaMaster QM, Photon Technology International, Edison NJ, USA). In the case of DOX, the UV-Visible spectrophotometer (Thermo Scientific Evolution 60S UV-Visible Spectrophotometer, Kobis Ltd., Slovenia) was used to measure the absorbance of DOX available in the sample, thus calculating the release efficiency.

The NH_2-Fe BDC MOF were prepared by following a previously published procedure [44] with some modifications: 54 mg of $FeCl_3.6(H_2O)$ and 36 mg of NH_2-BDC diluted in 5 mL of DMF. The solution was heated in a Temperature digestive microwave for 99 minutes under a power output of 8 watts and a temperature of 135 ^oC. Next, the resultant particles were separated by centrifugation for 15 minutes at 6000 rpm. Afterward, the solution was washed and centrifuged two times at the same conditions. The collected particles, namely NH_2-Fe BDC MOF, were dried in an oven at a temperature of 120 ^oC for 45 minutes. Then the product was stored for further modification.

3.4 Drug Encapsulation

To encapsulate the drug inside the MOFs, a PBS solution with a pH of 7 was prepared. 66.65 mg of calcein was added to 10 ml of PBS in order to obtain a 10-mM solution. Next, the pH of the solution was equilibrated to a value of 7.4 using HCl and NaOH. 15 mg of NH_2-Fe BDC MOFwere added to a 0.06-mM solution of calcein and placed on a stirrer for mixing. After 24 hours, the mixture was centrifuged for 30 minutes at 6000 rpm. Then, the supernatant was removed, and the drug-loaded MOFs were dried in an oven at a temperature of 100 ^oC for 1 hour. After the drying process, the drug-loaded MOFs were stored for further surface modification. In addition, a second study was conducted with loading the chemotherapeutic drug DOX. 15 mg of MIL-100 was added to a 1 mM DOX solution and the same procedure was carried out to produce DOX-loaded MOF. To calculate the drug loading efficiency, the following equation was used

$$loadig\ effiency = \frac{F_i - F_f}{F_f} * 100\% \quad (1)$$

where F_i and F_f are the fluorescence intensity of the initial and final calcein concentrations.

The same equation could be used in terms of the amount of DOX, where M_i and M_f are initial and final masses of DOX in the drug loading solution.

$$loadig\ effiency = \frac{M_i - M_f}{M_i} * 100\% \quad (2)$$

To measure the fluorescence intensity, two diluted samples were prepared. The first sample corresponds to the initial calcein concentration (F_i) prepared by diluting 70 µl of the 10-mM calcein solution with 5 ml of PBS. For the second sample (F_f), 70 µl of the supernatant was added to 5 ml of PBS. Next, a spectrofluorometer was used to measure the intensity of the fluorescence in each sample. The calcein fluorescence is detected at wavelengths from 490 to 515 nm. The loading capacity of the drug is measured using the following equation

$$Loading\ capacity = \frac{mass_{loaded}}{mass_{loaded} + mass_{MOF}} \quad (3)$$

where

$$mass_{loaded} = loading\ efficiency * initial\ mass\ of\ drug \quad (4)$$

And $mass_{MOF}$ is the mass of the unloaded MOF.

In this study, the surface of the synthesized NH_2-Fe BDC MOF was modified through post-synthesis modification steps to enhance targeting cancerous cells and reduce the side effects of the therapeutic drug on healthy cells. The synthesized MOF underwent surface functionalization by conjugating a PEG functional group and folic acid, resulting in folate-functionalized MOF samples. As discussed before, folic acid has a high affinity to folate receptors, which are overly expressed in breast cancer cells. The folate functionalization of the NH_2-Fe BDC MOFs step was performed as follows: 15 mg of the loaded NH_2- MOF was added to 10 ml of a solution of PEG-FA (0.75 mg), EDC (15mg), and NHS (30mg). Next, the mixture was incubated at room temperature for 3 hours. Finally, the samples were centrifuged, dried in an oven at 80 ^oC, and labeled as FA-NH_2-Fe BDC MOF. The conjugation is covered by a two-step reaction. First, the EDC reacts with the carboxylic group of the PEG, forming an unstable amine-reactive ester. Then, the addition of NHS stabilizes the ester, thus, enhancing its bonding efficiency. In the presence of an amine, the carboxylic group is attached to the positive amine group by substitution, removing the NHS/EDC ester.

3.5 Drug Release

Since the discovery of MOFs in 1998, a new class of MOFs has been identified as third-generation of functional MOFs. This new type of MOF is characterized by the dynamic, flexible features of the framework structure. Flexible MOFs can respond to

physical or chemical stimuli, including phase transition, mechanical, photochemical and thermal stimuli. Applying ultrasound on the MOF's particles will allow the chemical bonds to stretch and release the encapsulated chemical inside the pores. The ultrasound triggering mechanism was implemented to release the encapsulated calcein. Drug release experiments were conducted as follows: three batches of 15 mg of the loaded FA-NH_2-Fe BDC MOF were added to 5 ml of PBS at three different pH levels to produce an aqueous solution of the mixture. Calcein-loaded MOFs were set to release in PBS solutions of the following pHs 7.4, 6.4, 5 pH at a temperature of 37 ^oC. After applying low-frequency ultrasound (35 kHz) to the samples within a specific interval of time, the samples were centrifuged, and an aliquot was taken from the supernatant for analysis. At the same time, the same amount of the aliquot was replaced with fresh PBS for the next measurement. The physical effect of the ultrasound widens the pores of the MOF by stretching the chemical bonds between the metal cluster and the organic linker. This procedure was repeated until maximum release was reached. The calcein release studies served as a proof of concept for implementing ultrasound as a release stimulus. After the successful release study of calcein, two batches of DOX loaded MOFs were set to release at pHs of 7.4 and 5.3 in PBS, and one batch of PEG-folate MOF was set to release at a pH of 5.3 to study the effect of PEG functionalization on release efficiency. Furthermore, the effect of PEG-folate moiety on the release profiles with and without ultrasound, under two pH values (7.4 and 5.3) was studied.

To calculate the cumulative release efficiency, the following equation is used

$$cumulative\ release\ \ efficienc = \frac{Mass\ released}{maximum\ mass\ released} * 100\% \quad (5)$$

The amount of drug released for each run is calculated using a calibration curve, whether it is a florescence-concentration calibration curve (in the case of calcein) or an absorbance-concentration calibration curve (in the case of DOX).

Chapter 4. Results and Discussion

4.1 Characterization

4.1.1. FTIR. The FTIR spectra were measured using Spectrum one FT-IR spectrometer. Small amounts of the synthesized MOF were added to potassium bromide (200 mg). The mixture was grinded and then compressed under 3000 tons of uni-axial pressure. The produced disks were placed in the spectrometer for analysis. The spectrum of the synthesized MOF is shown in Figure 11-a. According to the plot, the amine functional can be seen at 2366- 3480 cm^{-1}. Moreover, the DMF used in the synthesis is shown at 1582 cm^{-1} and 1628 cm^{-1}. The N-H bond and C-N are shown at 1527 cm^{-1} and 1340 cm^{-1}, respectively.

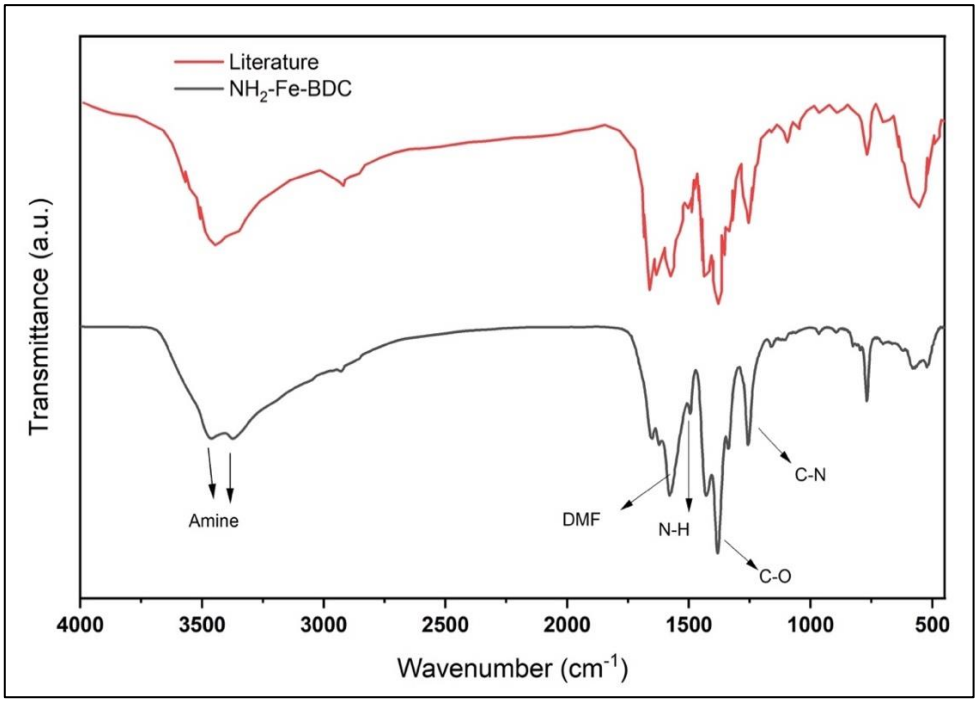

Figure 9:Figure 11:FTIR Analysis: a) FTIR of synthesized a) FA-NH2-Fe BDC MOF, b) FTIR of a FA-NH2-Fe BDC MOF [69]

The FTIR analysis conducted on the sample was to detect the functional groups present in the MOF structure. Comparing the results with data from literature [69] (Figure 11-b), the experimental results agree well with reported references and demonstrate similar peaks at the same wavelength, where each peak represents a specific chemical bond signifying the successful attachment of the folate functional group.

4.1.2. TGA. To analyze the thermal stability of the synthesized MOFs, thermogravimetric analysis (TGA) was performed. Figure 12 represents the weight loss % as a function of temperature for the MOF sample. The first reduction in weight (close to 20% wt. loss%) between room temperature and 300 ^{o}C corresponds to the removal of water moisture and DMF within the pores of the MOF samples, while the more pronounced weight loss % that appears in the temperature range of 300-500 is due to the decomposition of the MOF's framework. Comparing the results of the TGA analysis with literature (Figure 13), it can be seen that the experimental data is similar and follows the same graphical trend. The synthesized MOF starts degrading at 320 ^{o}C.

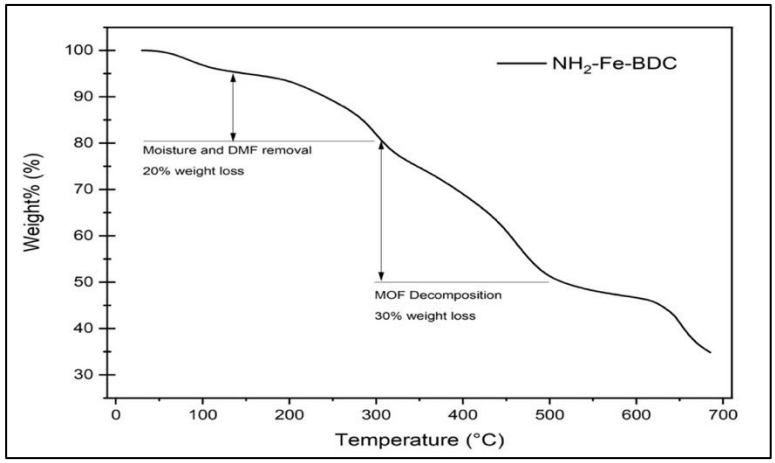

Figure 10:Percentage weight loss vs. temperature by TGA analysis

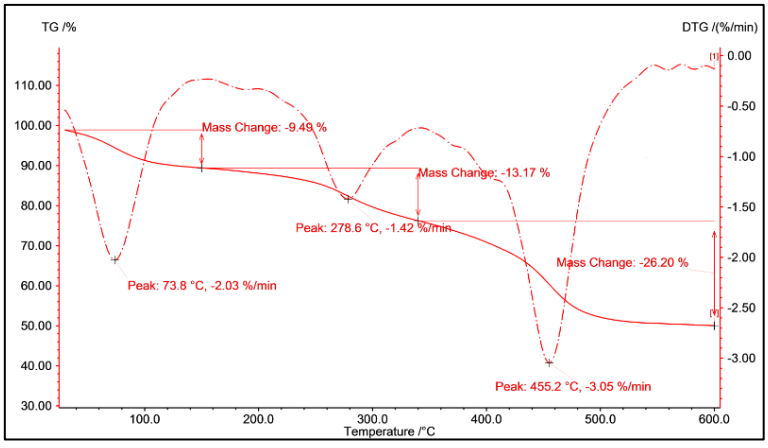

Figure 11: TGA of NH_2-Fe BDC MOF [70]

4.1.3. DLS. The Dynamic light scattering analysis was conducted using the DynaPro NanoStar dynamic light scattering unit by WYATT Technology. The analysis

resulted in a MOF diameter value of 215.6 nm Figure 14 which is suitable for *in vivo* studies [71].

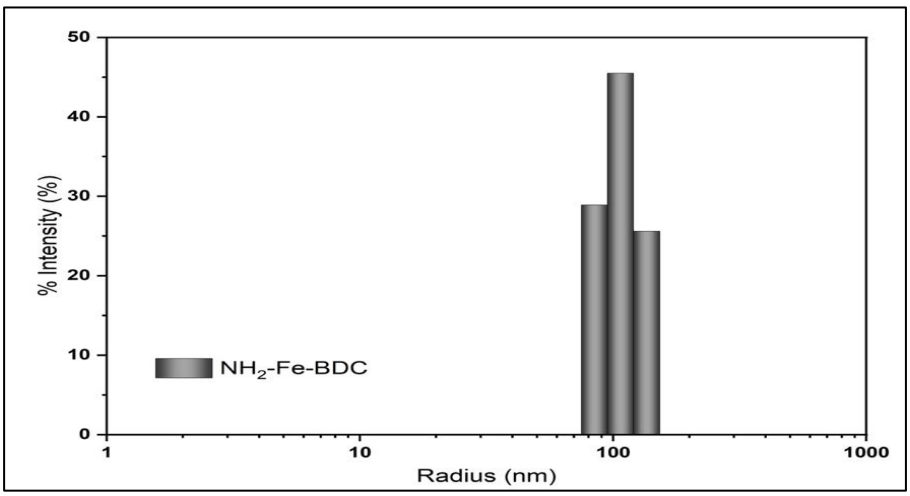

Figure 12:DLS analysis of NH_2-FE BDC MOF

4.1.4. XRD. The XRD analysis was conducted in the Engineering Labs at the University of Sharjah, Sharjah, United Arab Emirates. The XRD resulted in the graph showed in Figure 15-a. Compared with results from literature (Figure 15-b), it can be seen that the experimental data follows the same trend implying a successful synthesis of the NH_2-FE BDC MOF with the appropriate morphology.

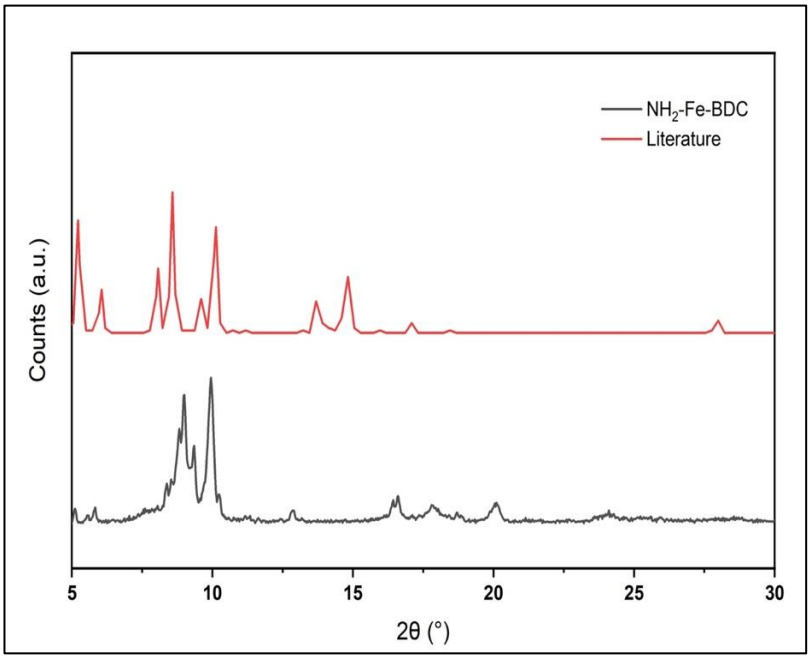

Figure 13:a) XRD analysis of the synthesized NH_2-FE BDC MOF b) XRD analysis of NH_2-FE BDC MOF [70]

4.1.5. SEM. The SEM analysis was done at the American University of Sharjah, Sharjah, United Arab Emirates. The analysis gives a visual image of the crystalline structure. The result of the SEM analysis is shown in figure 16-a. Compared with NH_2-FE BDC MOF SEM analysis from literature (Figure 16-b), it clearly shows that the synthesis was successful with the appropriate crystalline structure.

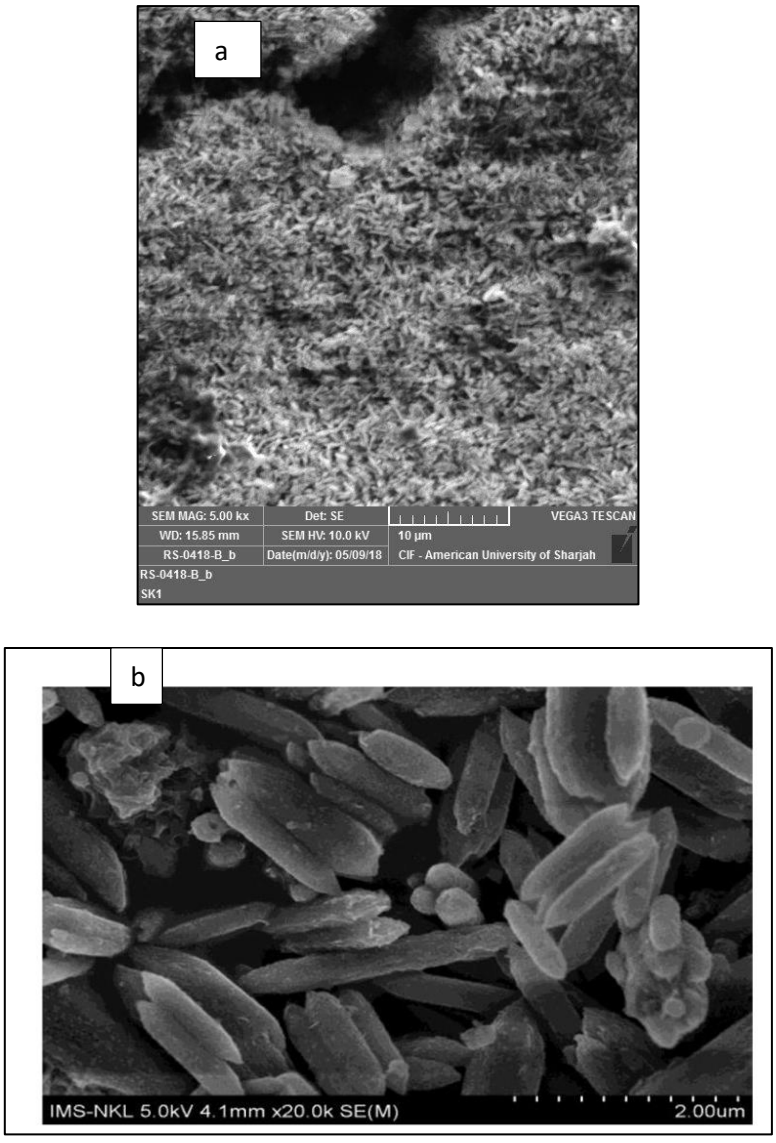

Figure 14: a) SEM analysis of the synthesized NH_2-FE BDC MOF b) SEM analysis of NH_2-FE BDC MOF[70]

4.2 Loading Efficiency

The initial solution was analyzed with the fluorometer to measure the loading efficiency of the NH_2-Fe BDC MOFMOF samples loaded with calcein. The average resulting intensity of the sample was 0.1853. After loading for 24 hours, a sample of the supernatant of the calcein mixture was analyzed by a fluorometer, resulting in an

average intensity of 0.036. According to Equation 1 proposed in section 4.4, the overall loading efficiency was around 90%. Moreover, in the case of DOX encapsulation, Equation 2 was used to calculate the loading efficiency for the DOX. The study resulted in a loading efficiency of around 97%.

4.3 Release Profiles

According to the procedure stated in section 4.5, cumulative efficiency release curves were plotted against time for both calcein- and DOX-loaded MOFs.

4.3.1. Calcein release profiles. As mentioned in the procedure, three batches of calcein-loaded MOFs were tested at three different pH conditions, i.e.,7.4, 6.4, and 5. Each sample was repeated three times resulting in a total of 9 trials. Figure 17 shows the cumulative release profiles at each pH level set during the experiments. All trials resulted in a high-efficiency release in a time period of almost two hours. As shown in Figure 17 a,b, and c, the trend is similar; the release percentages reached around 90%. This could be visually verified as the sample became transparent through time instead of being fluorescent, justifying the fact that almost all the drug adsorbed on the MOF was released.

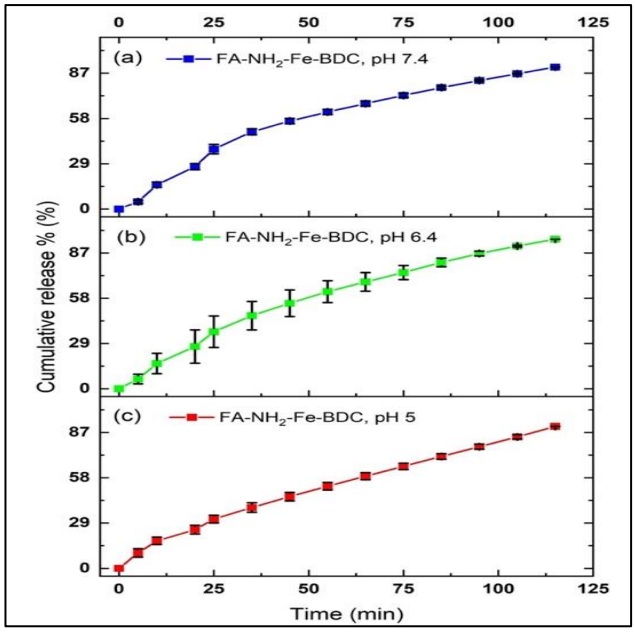

Figure 15:Cumulative release profiles of Calcein Loaded PEG-Folate MOF at a pH levels: a) 7.4, b) 6.4 and c) 5.3. The error bars indicating the standard deviation of three trials

4.3.2. DOX release profile. In the case of the DOX loaded MOFs, the experiments were conducted at two different pH conditions, including 7.4 and 5.3, for NH_2-Fe BDC MOF samples with and without ultrasound. Furthermore, to investigate the sonosensitivity of the functionalized MOF samples, release profiles of FA-NH_2-Fe BDC MOF were reported with and without ultrasound at pH 5.3. The effect of PEG-folate functionalization was studied at a pH of 5.3 since it simulates the tumor acidic microenvironment.

Figure 18 shows the average release profile of NH_2-Fe BDC MOF samples at pH 7.4. Three experiments were conducted for different batches of the loaded MOF. The study resulted in total release efficiencies of 42.9%, 43.7%, and 46.2%, with an average of 44.4 % in 4 hours and 40 minutes.

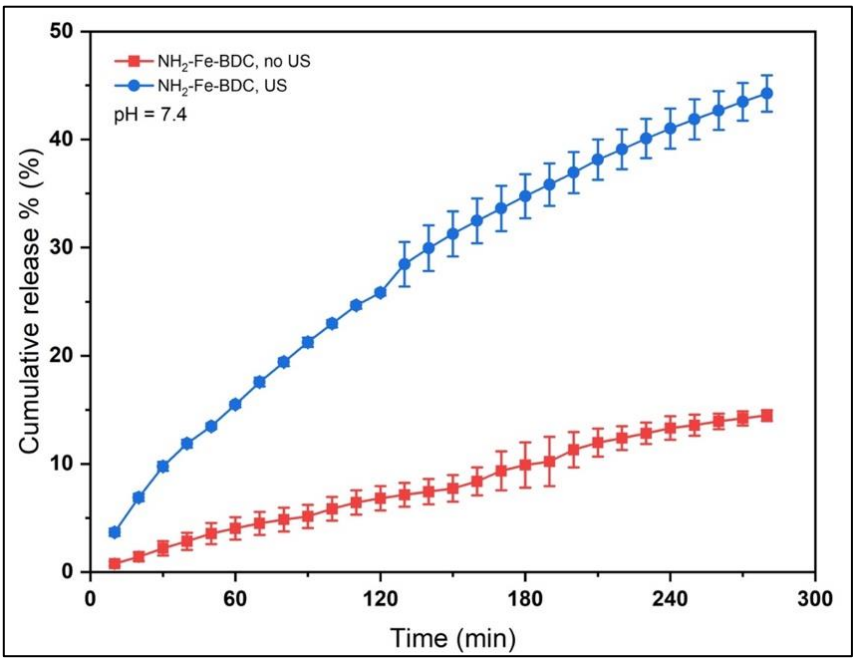

Figure 16: Cumulative release profiles for a DOX Loaded NH_2-Fe BDC MOF at a pH level of 7.4 with error bars indicating the standard deviation of three trials

Figure 19 shows the average release profile of the FA-NH_2-Fe BDC MOF trials in a PBS solution at a pH of 5.3. The three experiments resulted in total release efficiencies of 74.4%, 66.9%, and 69.3%, with an average of 70.2% over the same time period.

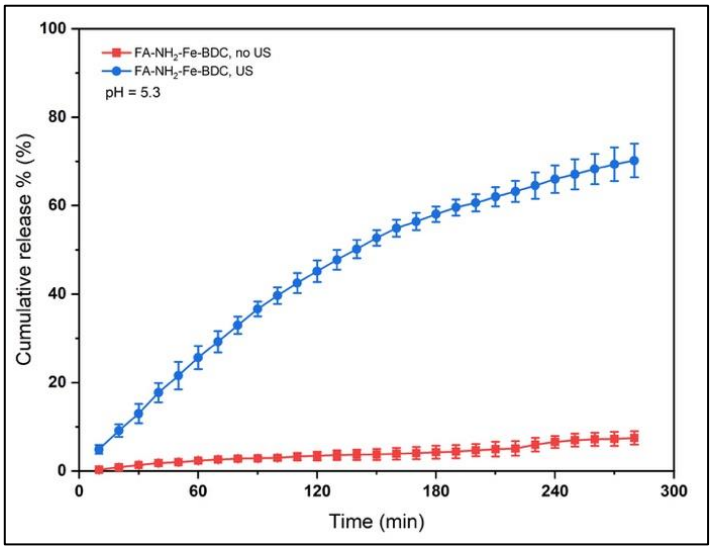

Figure 17: Cumulative release profiles of DOX Loaded FA-NH_2-Fe BDC MOF at a pH level of 5.3 with error bars indicating the standard deviation of three trials

Finally, Figure 20 shows the average release profiles of the NH_2-Fe BDC MOF trials in a PBS solution at a pH of 5.3. The three triplicates resulted in a total release of 88.7%, 86%, and 98%, with an average of 90.9% over the same period.

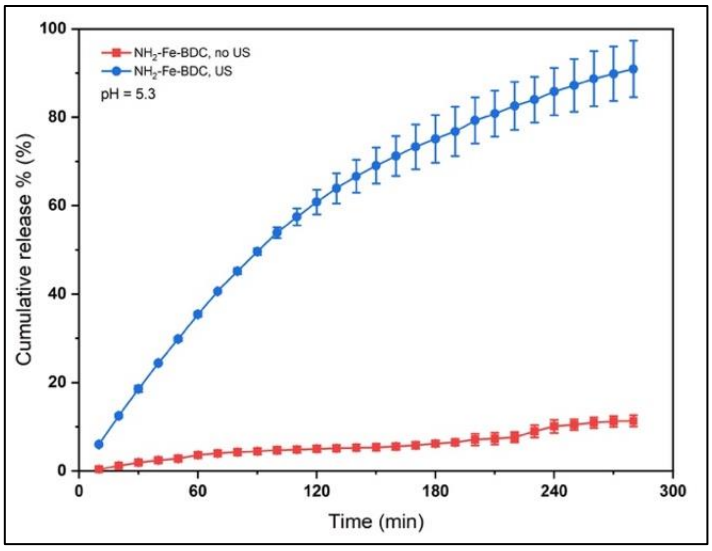

Figure 18: Cumulative release profiles of DOX Loaded NH_2-Fe BDC MOF at a pH level of 5.3 with error bars indicating the standard deviation of three trials

As can be seen, the highest cumulative release percentage (~ 90%) was achieved using the NH_2-Fe BDC MOF samples at a pH of 5.3, while the lowest percentage corresponded to the NH_2-Fe BDC MOF samples at a pH value of 7.4. It can be deduced that the release is much more effective at low pH values, which is

preferable since the cancerous or tumor environment is more acidic compared to healthy tissue [72]. Moreover, in comparison with the release from FA-NH_2-Fe BDC MOF samples conducted at the same pH, it was noticed that the functionalized MOF resulted in a lower release percentage than the unfunctionalized NH_2-Fe BDC MOF. This decrease in the release percentage is due to the fact that MOF loading /release capacities depend on their surface morphology, and as functionalization modifies the surface of the MOF, it would be more difficult for the drug to escape or get released from the surface.

4.4 Kinetic Release Modeling:

Mathematical modeling gives a prediction of the release kinetics of a system. It also allows determining certain parameters. For example, in the case of drug delivery systems, modeling aids the calculation of drug diffusion coefficients and other physical parameters alongside having a major role in process optimization. As mentioned above, the releases kinetics of the loaded MOF were fitted to nine drug release models (Table 1).

Table 1: Drug Delivery Release Models

Model	Equation
Higuchi model[73]	$Q = A\sqrt{D(2C - C_S)C_s t}$
Zero-order[73]	$Q_t = Q_0 + K_0 t$
First-order[74]	$\log C = \log C_0 - Kt/2.303$
Baker-Lonsdale model[73]	$\frac{3}{2} * \left[1 - \left(1 - \frac{M_t}{M_\infty}\right)^{\frac{2}{3}}\right] \frac{M_t}{M_\infty} = K_t$
Weibull model[75]	$M = M_0[1 - e^{-\frac{(t-T)^b}{a}}]$
Korsmeyer-Peppas[76]	$M_t/M_\infty = k\ t^n$
Hixson-Crowell[75]	$w_o^{\frac{1}{3}} - w_t^{\frac{1}{3}} = k\ t$
Hopfenburg model[77]	$\frac{M_t}{M_\infty} = 1 - [1 - \frac{k_0 t}{C_L a}]^n$
Gomperts model[78]	$X_t = X_{max} \exp[-\alpha e^{\beta \log t}]$

Higuchi model: the Higuchi model was proposed in 1961 to describe the behavior of drug release from matrix systems. The model was based on assumptions that the initial concentration is higher than the solubility, that one-directional release, constant diffusivity, drug particles are smaller than the system thickness, and that negligible matrix swelling and dissolution occurred. The model is expressed by

$$Q = A\sqrt{D(2C - C_S)C_s t} \tag{6}$$

where Q is the rate of drug release, A is the unit area, D is the diffusivity, C is the initial drug concentration, and C_s is the drug solubility [73].

Zero-order Release Model: The drug release follows zero-order kinetics, which refers to a constant slow release expressed by the following equation:

$$Q_t = Q_0 + K_0 t \tag{7}$$

where Q_t is the amount of drug release, Q_0 is the initial amount of drug in the solution, and K_0 is the zero-order release constant [73].

First-order Release Model: The release follows first-order kinetics expressed by the following equation:

$$\log C = \log C_0 - Kt/2.303 \tag{8}$$

where C and C_0 represent the concentration of the drug at a specific interval of time and the initial concentration, respectively, K is the first-order constant, and t is time. The model is used to describe water-soluble drugs in porous material [73], [74].

The Baker-Lonsdale model: This model was developed from the Higushi model in 1974 and is expressed in the following equation:

$$\frac{3}{2} * \left[1 - \left(1 - \frac{M_t}{M_\infty}\right)^{\frac{2}{3}}\right] \frac{M_t}{M_\infty} = K_t \tag{9}$$

where M is the amount of drug released at a specific time (t), and K is the release constant. The model was developed to serve or predict the release of spherical or capsule-like material [73].

The Weibull model: The model is used to describe various dissolution processes as expressed through the following equation:

$$M = M_0[1 - e^{-\frac{(t-T)^b}{a}}] \quad (10)$$

where *M* is the amount of drug released as a function of time, M_0 is the total amount of drug being released, *T* accounts for lag time, *a* denotes a scale parameter that describes the time dependence, while *b* describes the shape of the dissolution curve progression. The model best describes matrix drug delivery systems [75].

Korsmeyer-Peppas model: This model was developed in 1983 to describe the release profile of polymeric delivery systems. The model is expressed by the following equation:

$$\frac{M_t}{M_\infty} = kt^n \quad (11)$$

where M_t/M_∞ is the fraction of drug released at a specific interval of time to the total amount being released, k is the release rate constant, and n is the release exponent, which characterizes different release mechanisms [76].

Hixson-Crowell: This model was developed on the basis that the particle regular area is proportional to the cube root of its volume. The model is expressed by the following equation:

$$w_o^{\frac{1}{3}} - w_t^{\frac{1}{3}} = k\,t \quad (12)$$

where w_o and w_t are the initial amount of drug in the dosage and the remaining amount of drug in the dosage, respectively, k is the surface/volume constant, and t is time. The model describes the release from tablets or particles where there is a change in surface area and diameter through time, such as the dissolution of pharmaceutical tablets [75].

Hopfenburg model: This model was developed to describe the controlled release from surface eroding polymers of constant surface area. The model is expressed by the following equation:

$$\frac{M_t}{M_\infty} = 1 - [1 - \frac{k_0 t}{C_L a}]^n \quad (13)$$

where M_t/M_∞ is the cumulative drug release fraction, k_0 is the erosion rate constant for surface erosion, C_L is the initial drug loading amount, a is the half-thickness of the system, and n corresponds to the geometry of the system[73], [77].

Gomperts model: Gompertz exponential model usually describes *in vitro*. The model is expressed via the following equation:

$$X_t = X_{max} \exp\left[-\alpha e^{\beta \log t}\right] \quad (14)$$

where X_t and X_{max} are drug release percent, and the maximum amount of drug released, respectively, α determines the undissolved proportion at t=1 (scale parameter), β dissolution rate (a shape parameter). The model demonstrates a release pattern in which a steep release profile is followed by a slow convergence to the maximum amount of the loaded drug [78], [79].

4.4.1. Calcein kinetic release models. The data of calcein release from MOF's were fitted to the models mentioned above. Each data sample was fitted to nine models. Each model represents the drug release from a certain drug carrier system of specific form of drug. Different factors may affect the drug release kinetics, The Type of carrier i.e. porous materials, matrix degrading systems, surface eroding systems (pharmaceutical pills), circular and capsule like systems. Moreover the chemical properties of the pharmaceutical or chemotherapeutic drug plays a role in determining the release kinetics of the system. Properties such as water solubility and polarity are taken into consideration. Next, a regression analysis was conducted as a measure of how well the data fit the linearized form of the models. The R^2 values of each model fit are shown in Table 2. For FA-NH_2-Fe BDC, MOF at a pH of 7.4 showed the highest R^2 value, which resulted from the Weibull model fitting which represents the drug release of various dissolutions systems or release form pharmaceutical dosage forms such as matrix type drug delivery systems. The regression value was recorded to be 0.9934. As for FA-NH_2-Fe BDC MOF@pH 6.4, the highest R^2 value was recorded for the Korsmeyer-Peppas model which represents the release from a polymeric drug delivery system with a value of 0.9955. Finally, the highest R^2 value for sample FA-NH_2-Fe BDC MOF@pH 5 was recorded from the zero-order Model fitting which represent a slow controlled release following first order kinetics of a matrix type carriers with a value of 0.9924.

Table 2: Calcein samples R-squared values

MODEL	PEG-folate-MOF@pH7.4	PEG-folate-MOF@pH6.4	PEG-folate-MOF@pH5
Higuchi model	0.9907	0.987	0.9638
Zero-order	0.9347	0.9635	0.9924
First-order	0.6756	0.7445	0.8616
Baker-Lonsdale	0.9781	0.9473	0.9117
Weibull	0.9934	0.9929	0.9728
Korsmeyer-Peppas	0.9885	0.9955	0.9814
Hixson-Crowell	0.9923	0.9903	0.9803
Hopfenberg	0.9923	0.9903	0.9803
Gompertz	0.9377	0.8719	0.8525

4.4.2. DOX kinetic release models. Similarly, a regression analysis was conducted for the data recorded using the DOX-loaded MOFs samples. The R^2 value was recorded for each of the nine models and is shown in Table 3. For DOX-NH_2-Fe BDC MOF@pH 7.4, the highest R^2 value was calculated using the Korsmeyer-Peppas Model with a value of 0.9975, while for DOX-PEG-folate- MOF@pH5.3, the highest R^2 value was recorded using both the Hixon-Crowell and Hopfenburg models with a

value of 0.999. Finally, the highest R^2 value for DOX-NH_2-Fe BDC MOF@pH 5.3 was recorded using the Baker-Lonsdale model with a value of 0.9938.

Table 3:DOX samples R-squared values

MODEL	DOX-NH2-MOF@7.4	DOX-PEG-folate-MOF@pH5.3	DOX-NH2-MOF@pH5.3
Higuchi	0.997	0.9937	0.9925
Zero-order	0.9772	0.9457	0.9417
First-order	0.8147	0.7648	0.735
Baker-Lonsdale	0.9862	0.9775	0.9938
Weibull	0.9938	0.999	0.9866
Korsmeyer-Peppas	0.9975	0.983	0.9782
Hixson-Crowell	0.9935	0.9991	0.9873
Hopfenberg	0.9935	0.9991	0.9873
Gompertz	0.984	0.9297	0.9846

As mentioned, many structures were utilized as nano-drug carriers for many types of diseases and health issues such as cancer, diabetes, inflammation, and even pain relief.. Liposomes were the first drug delivery vehicle to get FDA approval in 1995. A study by Li et al. demonstrated the application of liposomes in drug delivery; the chemotherapeutic drug DOX was encapsulated by liposomes and set to be used to

treat MCF-7 cells. The study showed a loading efficiency of around 80%, and release efficiency of around 50% for release at a pH of 5, 40% at a pH of 6.5, and 38% at a pH of 7.4. The study was conducted over a period of 72 hours [80].

Moreover, a study by Cheng et al. demonstrated the application of folate-PEG functionalized liposomes in drug delivery. The study tested the release of DOX at two different pH environments 7.4 and 6.4, and two different temperatures, 37 and 42 °C. The loading efficiency of both samples ranged between 68% to 75% at both pH conditions. Release at a pH of 7.4, and the two investigated temperatures, namely 37 and 42 °C, was 15% and 50%, respectively. Meanwhile, the release at a pH of 6.4 resulted in a release efficiency of 20 % and 60%, with the highest release corresponding to the highest temperature. The release was conducted over a period of 5 hours [81].

In addition, Bi et al. studied the utilization of liposomes as drug carriers. The study used DOX as the loaded drug. The release of the drug from liposomes was tested in three environments with different pH levels, i.e., 7.4, 6.5, and 5. The encapsulation efficiency was recorded around 91% for all samples. The study resulted in the release percentages of 70%, 58%, and 30%, with the lowest pH level having the highest release percentage. The study was conducted over 120 hours [82].

In addition to liposomes, Polymeric micelles were also utilized as drug nanocarriers in many studies. Polymeric micelles are single bilayer phospholipids that encapsulate chemical agents into their hydrophobic core. Chemotherapeutic drugs such as DOX were encapsulated inside the polymeric structures. A study by Zhang et al. utilized pH-responsive micelles as DOX nano-carriers. The study showed a loading capacity of 50.3%. The release testing was performed in two environments of different pH levels of 7.4 and 5. The results showed a cumulative release percentage of around 58% at a pH level of 5 and 11% at a pH level of 7.4. The test was conducted over 90 hours [83].

Moreover, Xiong et al. demonstrated the use of micelles in drug delivery and CT imaging applications. Redox-sensitive micelles were synthesized by the self-assembly of polymers. The chemotherapeutic drug was encapsulated inside the core of the micelles. The study resulted in an encapsulation efficiency of 48.4%. The release of DOX was investigated at two different simulated physiological conditions of

different pH levels. At a pH level of 7.4, the release study resulted in a maximum release percentage of 29.9%, while at a pH of 5, the study resulted in a maximum release of 73.1%. The release study was conducted for 36 hours [84].

In addition, a study by Lu et al. also demonstrated the use of targeted micelles in drug delivery. The polymeric-based micelles were synthesized by self-assembly. The chemotherapeutic drug was encapsulated inside the core of micelles resulting in an encapsulation efficiency of 47.16%. The drug was set to be released in two simulated environments of different pH levels; 7.4 and 5. The release measured at a pH level of 7.4 resulted in a maximum release percentage of around 30%, while in the case of the release at a pH of 5, the study resulted in a maximum release percentage of ~60%. The study was conducted over 50 hours [85].

Furthermore, pH is an internal drug release stimulus. Many studies utilized pH-sensitive MOFs for drug delivery applications. At acidic conditions, the coordination bonds breakdown while decomposing or degrading the MOF, thus releasing the encapsulated drug [86].

For example, Gupta *et al.* developed a bio-compatible iron-based MOF to be utilized as a pH-responsive drug delivery system. The synthesized MOF was coated with PEG through post-synthesis amine modification. The drug Ibuprofen was loaded into both the PEGylated and the non-PEGylated MOFs for release studies. The release profiles were obtained at 3 different pH levels 7.4, 6 and 5. Ibuprofen sustained release was observed to be 57.52% and 46.05% after 20 h at a pH 7.4 from NH_2-MIL-101-Fe and PEG@Drug@NH2-MIL-101-Fe, respectively. While at pH 6, the release percentage was 69.09% and 42.3%, and at pH 5 the release percentage was 74.25% and 52% [87].

Moreover, another study by Garcia et al. utilized the iron-based MOFs MIL-100 and MIL 101 as a pH-sensitive drug delivery nanocarriers. The chemotherapeutic drug camptothecin was encapsulated in the MOF by covalent bonding. MTT assays were conducted to determine the cytotoxic effect of the MOF. The MTT was conducted on HeLa cell line, resulting in above 80% cell viability. The loading of the chemotherapeutic drug camptothecin resulted in a loading capacity of 20 % wt. The release study was conducted at three pH conditions 7.4, 5, and 3. The study resulted in release efficiencies of 12%, 25%, and 28 %, respectively, after 48 hours [88].

Last but not least, Lin et al. investigated the performance of MIL-100 toward doxorubicin encapsulation and release under pH effect. The MOF was characterized using XRD, IR, SEM and TEM. MTS assays were conduct to determine the cytotoxicity of the nano-particles. The cytotoxicity assay were conducted on a MDF-7 cell line and resulted in above 80% cell viability suggesting that the MOFS have a low cytotoxic effect. The drug loading concentration was 50 mg/g_{MOF}. The Release study was conducted at two different pH levels. The study resulted in 100% release efficiency after 60 hours at a pH of 3.8 and a 20% release efficiency at a pH of 7.4 after 50 hours [89].

In comparison with the aforementioned studies, it can be concluded that ultrasound had a significant effect on the release efficiencies and profiles compared to the other release triggering mechanisms. Implementing ultrasound as a release stimulus resulted in a maximum of 90% release efficiency for the DOX loaded NH_2-Fe BDC MOF within 5 hours at a pH 5.3. The physical effect of the ultrasound allows the MOF's pores to widen by stretching its chemical bonds, thus releasing the encapsulated drug or compound.

Table 4 shows the comparison between the MOF used in this study and nano-drug carriers from literature in terms of loading capacity, maximum release percent, and experimentation period. All moieties listed were used to encapsulate the chemotherapeutic drug DOX and the release was investigated at a neutral pH(7.4) and an acidic pH(5.3). As shown in Table 4, the MOF moiety showed the highest loading efficiency of 97% compared to the other mentioned moieties i.e. Liposomes and polymeric Micelles. Given that MOFs possess a highly porous structure, they able to adsorb a large amount of adsorbents or absorb chemical compounds into their molecular void compared to its weight. Moreover, the MOF's release percentage was the most effective compared to other nano-drug carrier systems, having a release percentage of 44.2% in a neutral environment and a 90.9% in an acidic environment in just 5 hours.

Table 4: Nano-Drug Carriers Comparison

Study	Moiety	Loading Capacity (%)	pH level	Maximum Release percentage	Time (hours)
Li et al. [78]	Liposomes	80%	7.4	38%	72
			5	50%	
Chang et al. [79]	Liposomes	68-75 %	7.4	15%	5
			6.4	20%	
Bi et al.[80]	Liposomes	91%	7.4	30%	120
			5	70%	
Zhang et al. [81]	Micelles	50.3%	7.4	11%	90
			5	58%	
Xiong et al. [82]	Micelles	48.4%	7.4	29.9%	36
			5	73.1%	
Lu et al. [83]	Micelles	47.16%.	7.4	30%	50
			5	60%	
NH_2-BDC-MOF This study		97%	7.4	44.2%	5
			5.3	90.9%	

Chapter 5. Conclusions and Future Work

In conclusion, an iron-based NH_2-Fe BDC MOF was successfully synthesized using microwave-assisted synthesis to be utilized for drug delivery applications by implementing ultrasound as a release triggering mechanism. In addition, PEG-folate functionalization was incorporated onto the surface of the MOF, using a post-synthesis modification technique, as a cancer biomarker targeting ligand. Several characterization tests were performed, including FTIR, TGA, and DLS to analyze the morphology, thermal stability, and particle size distribution of the MOF samples. The results of the characterization tests showed the successful synthesis, and the successful PEG-folate attachment, in addition to the excellent thermal stability and a suitable particle diameter for *in vitro* and *in vivo* applications. The model drug calcein and the chemotherapeutic drug DOX are successfully adsorbed on the MOF structure. The MOF achieved a suitable loading efficiency of 90% in the case of calcein and 97% in the case of DOX. The use of ultrasound was implemented as an external release stimulus. Release profiles were obtained for both the calcein and DOX encapsulation. The release of the model drug calcein was performed in 7.4-, 6.4- and 5-pH PBS solutions resulting in a release efficiency of 90% under US. While, release profiles for the DOX encapsulation resulted in cumulative release efficiencies of 44.4 % and 90% in 7.4- and 5.3-pH PBS solutions under US, respectively. Moreover, the PEG-Folate functionalization was investigated as a targeting mechanism for cancerous tissues in conditions mimicking the tumor microenvironment; the release profile of the FA-NH_2-Fe BDC MOF resulted in maximum release efficiency of 70.2% at a 5.3 pH PBS solution. The release profiles were fitted into nine drug release models along with a regression analysis study. The results reported in this thesis has shown the effectiveness of metal organic frameworks as promising drug carrier candidates for cancer treatment.

Based on this thesis and its experimental results, it is recommended to investigate the *in vitro* cell studies using the MCF-7 cell line along with flow cytometry analysis for both NH_2-Fe BDC MOF and the FA-NH_2-Fe BDC MOF with and without US. Furthermore, it is recommended to conduct *in vivo* animal studies to monitor the effectiveness of the FA-NH_2-Fe BDC MOF in cancer cells apoptosis and tumor volume reduction

References

[1] "Surgery", *National Cancer Institute*, 2018. [Online]. Available: https://www.cancer.gov/about-cancer/treatment/types/surgery. [Accessed: 18- Feb- 2018].

[2] M. H. Abdel-Kader, *Photodynamic therapy: from theory to application*. Berlin, Springer, 2014.

[3] "Radiation Therapy", *National Cancer Institute*, 2018. [Online]. Available: https://www.cancer.gov/about-cancer/treatment/types/radiation-therapy. [Accessed: 18- Feb- 2018].

[4] R. Skeel and S. Khlief, *Handbook of Cancer Chemotherapy*. Philadelphia: Wolters Kluwer, 2015.

[5] S. Svenson, "*Carrier-Based Drug Delivery*, 5th ed", ACS Publications, 2004, pp. 2–23.

[6] L. Sercombe, T. Veerati, F. Moheimani, S. Y. Wu, A. K. Sood, and S. Hua, "Advances and challenges of liposome assisted drug delivery," *Frontiers in Pharmacology*, vol. 6, no. DEC. Frontiers Media S.A., p. 286, 01-Dec-2015.

[7] Z. Wang, X. Deng, J. Ding, W. Zhou, X. Zheng and G. Tang, "Mechanisms of drug release in pH-sensitive micelles for tumour targeted drug delivery system: A review", *International Journal of Pharmaceutics*, vol. 535, no. 1-2, pp. 253-260, 2018.

[8] Y. Yi, G. Lin, S. Chen, J. Liu, H. Zhang and P. Mi, "Polyester micelles for drug delivery and cancer theranostics: Current achievements, progresses and future perspectives", *Materials Science and Engineering: C*, vol. 83, pp. 218-232, 2018.

[9] H. Zhou, J. Long and O. Yaghi, "Introduction to Metal–Organic Frameworks", *Chemical Reviews*, vol. 112, no. 2, pp. 673-674, 2012.

[10] S. Beg, M. Rahman, A. Jain, S. Saini, P. Midoux, C. Pichon, F. Ahmad and S. Akhter, "Nanoporous metal organic frameworks as hybrid polymer–metal composites for drug delivery and biomedical applications", *Drug Discovery Today*, vol. 22, no. 4, pp. 625-637, 2017.

[11] S. Keskin and S. Kızılel, "Biomedical Applications of Metal Organic Frameworks", *Industrial & Engineering Chemistry Research*, vol. 50, no. 4, pp. 1799-1812, 2011.

[12] J. Perry, J. Perman and M. Zaworotko, "ChemInform Abstract: Design and Synthesis of Metal-Organic Frameworks Using Metal-Organic Polyhedra as Supermolecular Building Blocks", *ChemInform*, vol. 40, no. 29,pp. 1400-1417, 2009.

[13] P. Horcajada, C. Serre, G. Maurin, N. Ramsahye, F. Balas, M. Vallet-Regí, M. Sebban, F. Taulelle and G. Férey, "Flexible Porous Metal-Organic Frameworks for a Controlled Drug Delivery", *Journal of the American Chemical Society*, vol. 130, no. 21, pp. 6774-6780, 2008.

[14] T. Bennett and A. Cheetham, "Amorphous Metal–Organic Frameworks", *Accounts of Chemical Research*, vol. 47, no. 5, pp. 1555-1562, 2014.

[15] R. Huxford, J. Della Rocca and W. Lin, "Metal–organic frameworks as potential drug carriers", *Current Opinion in Chemical Biology*, vol. 14, no. 2, pp. 262-268, 2010.

[16] W. Rieter, K. Taylor and W. Lin, "Surface Modification and Functionalization of Nanoscale Metal-Organic Frameworks for Controlled Release and Luminescence Sensing", *Journal of the American Chemical Society*, vol. 129, no. 32, pp. 9852-9853, 2007.

[17] K. Mocniak, I. Kubajewska, D. Spillane, G. Williams and R. Morris, "Incorporation of cisplatin into the metal–organic frameworks UiO66-NH2 and UiO66 – encapsulation vs. conjugation", *RSC Advances*, vol. 5, no. 102, pp. 83648-83656, 2015.

[18] C. McGuire and R. Forgan, "ChemInform Abstract: The Surface Chemistry of Metal-Organic Frameworks", *ChemInform*, vol. 46, no. 21, pp. 5199-5217, 2015.

[19] S. Wuttke, M. Lismont, A. Escudero, B. Rungtaweevoranit and W. Parak, "Positioning metal-organic framework nanoparticles within the context of drug delivery – A comparison with mesoporous silica nanoparticles and dendrimers", *Biomaterials*, vol. 123, pp. 172-183, 2017.

[20] N. Stock and S. Biswas, "ChemInform Abstract: Synthesis of Metal-Organic Frameworks (MOFs): Routes to Various MOF Topologies, Morphologies, and Composites", *ChemInform*, vol. 43, no. 16, pp. 933-969, 2012.

[21] N. Stock and S. Biswas, "Synthesis of Metal-Organic Frameworks (MOFs): Routes to Various MOF Topologies, Morphologies, and Composites", *Chemical Reviews*, vol. 112, no. 2, pp. 933-969, 2011.

[22] "Microwave Synthesis of a Nanoporous Hybrid Material, Chromium Trimesate", *Bulletin of the Korean Chemical Society*, vol. 26, no. 6, pp. 880-881, 2005.

[23] R. Vakili, S. Xu, N. Al-Janabi, P. Gorgojo, S. Holmes and X. Fan, "Microwave-assisted synthesis of zirconium-based metal organic frameworks (MOFs): Optimization and gas adsorption", *Microporous and Mesoporous Materials*, vol. 260, pp. 45-53, 2018.

[24] BartłomiejSzyja, E. Pidko, R. Groote, E. Hensen and R. Sijbesma, "DFT Study on mechanochemical bond breaking in COGEF and Molecular Dynamics simulations", *Procedia Computer Science*, vol. 4, pp. 1167-1176, 2011.

[25] Y. Yoo and H. Jeong, "Rapid fabrication of metal organic framework thin films using microwave-induced thermal deposition", *Chemical Communications*, no. 21, p. 2441, 2008.

[26] N. Singh, S. Gupta, V. Pecharsky and V. Balema, "Solvent-free mechanochemical synthesis and magnetic properties of rare-earth based metal-organic frameworks", *Journal of Alloys and Compounds*, vol. 696, pp. 118-122, 2017.

[27] Y. Chen, J. Xiao, D. Lv, T. Huang, F. Xu, X. Sun, H. Xi, Q. Xia and Z. Li, "Highly efficient mechanochemical synthesis of an indium based metal-organic framework with excellent water stability", *Chemical Engineering Science*, vol. 158, pp. 539-544, 2017.

[28] T. Shono, *The New Chemsitry*. Cambridge University Press, 2000, pp. 55-85, chapter 4.

[29] J. Bang and K. Suslick, "Applications of Ultrasound to the Synthesis of Nanostructured Materials", *Advanced Materials*, vol. 22, no. 10, pp. 1039-1059, 2010.

[30] M. Bigdeli and A. Morsali, "Sonochemical synthesis of a nano-structured zinc(II) amidic pillar metal–organic framework", *Ultrasonics Sonochemistry*, vol. 27, pp. 416-422, 2015.

[31] M. Gharib, V. Safarifard and A. Morsali, "Ultrasound assisted synthesis of amide functionalized metal-organic framework for nitroaromatic sensing", *Ultrasonics Sonochemistry*, vol. 42, pp. 112-118, 2018.

[32] X. Gao, R. Cui, G. Ji and Z. Liu, "Size and surface controllable metal–organic frameworks (MOFs) for fluorescence imaging and cancer therapy", *Nanoscale*, vol. 10, no. 13, pp. 6205-6211, 2018. Available: 10.1039/c7nr08892b [Accessed 22 November 2020].

[33] M. Sajid, "Toxicity of nanoscale metal organic frameworks: a perspective", *Environmental Science and Pollution Research*, vol. 23, no. 15, pp. 14805-14807, 2016.

[34] F. Novio, J. Simmchen, N. Vázquez-Mera, L. Amorín-Ferré and D. Ruiz-Molina, "Coordination polymer nanoparticles in medicine", *Coordination Chemistry Reviews*, vol. 257, no. 19-20, pp. 2839-2847, 2013.

[35] A. Ma, Z. Luo, C. Gu, B. Li and J. Liu, "Cytotoxicity of a metal–organic framework: Drug delivery", *Inorganic Chemistry Communications*, vol. 77, pp. 68-71, 2017.

[36] I. Vasconcelos, T. Silva, G. Militão, T. Soares, N. Rodrigues, M. Rodrigues, N. Costa, R. Freire and S. Junior, "Cytotoxicity and slow release of the anti-cancer drug DOX from ZIF-8", *RSC Advances*, vol. 2, no. 25, p. 9437, 2012.

[37] T. Baati, L. Njim, F. Neffati, A. Kerkeni, M. Bouttemi, R. Gref, M. Najjar, A. Zakhama, P. Couvreur, C. Serre and P. Horcajada, "In depth analysis of the in vivo toxicity of nanoparticles of porous iron(iii) metal–organic frameworks", *Chemical Science*, vol. 4, no. 4, p. 1597, 2013.

[38] R. S. Forgan, "Metal-Organic Frameworks: Edible Frameworks," in *Encyclopedia of Inorganic and Bioinorganic Chemistry*, Chichester, UK: John Wiley & Sons, Ltd, 2014, pp. 1–13.

[39] K. Taylor, W. Rieter and W. Lin, "Manganese-Based Nanoscale Metal−Organic Frameworks for Magnetic Resonance Imaging", *Journal of the American Chemical Society*, vol. 130, no. 44, pp. 14358-14359, 2008.

[40] J. Zhuang, C. Kuo, L. Chou, D. Liu, E. Weerapana and C. Tsung, "Optimized Metal–Organic-Framework Nanospheres for Drug Delivery: Evaluation of Small-Molecule Encapsulation", *ACS Nano*, vol. 8, no. 3, pp. 2812-2819, 2014.

[41] C. He, K. Lu, D. Liu and W. Lin, "Nanoscale Metal–Organic Frameworks for the Co-Delivery of Cisplatin and Pooled siRNAs to Enhance Therapeutic Efficacy in Drug-Resistant Ovarian Cancer Cells", *Journal of the American Chemical Society*, vol. 136, no. 14, pp. 5181-5184, 2014.

[42] "Coordination polymer particles as potential drug delivery systems", *Chemical Communications*, vol. 46, no. 26, p. 4737, 2010.

[43] M. Rowe, D. Thamm, S. Kraft and S. Boyes, "Polymer-Modified Gadolinium Metal-Organic Framework Nanoparticles Used as Multifunctional Nanomedicines for the Targeted Imaging and Treatment of Cancer", *Biomacromolecules*, vol. 10, no. 4, pp. 983-993, 2009.

[44] J. Liu, L. Zhang, J. Lei, H. Shen and H. Ju, "Multifunctional Metal–Organic Framework Nanoprobe for Cathepsin B-Activated Cancer Cell Imaging and Chemo-Photodynamic Therapy", *ACS Applied Materials & Interfaces*, vol. 9, no. 3, pp. 2150-2158, 2017.

[45] C. Ding, L. Tong, J. Feng and J. Fu, "Recent Advances in Stimuli-Responsive Release Function Drug Delivery Systems for Tumor Treatment", *Molecules*, vol. 21, no. 12, p. 1715, 2016.

[46] "Redox-responsive polymers for drug delivery: from molecular design to applications", *Polym. Chem.*, vol. 5, no. 5, pp. 1519-1528, 2014.

[47]R. Abazari, A. Reza Mahjoub, A. Slawin and C. Carpenter-Warren, "Morphology- and size-controlled synthesis of a metal-organic framework under ultrasound irradiation: An efficient carrier for pH responsive release of anti-cancer drugs and their applicability for adsorption of amoxicillin from aqueous solution", *Ultrasonics Sonochemistry*, vol. 42, pp. 594-608, 2018.

[48] C. Sun, C. Qin, X. Wang, G. Yang, K. Shao, Y. Lan, Z. Su, P. Huang, C. Wang and E. Wang, "Zeolitic imidazolate framework-8 as efficient pH-sensitive drug delivery vehicle", *Dalton Transactions*, vol. 41, no. 23, p. 6906, 2012.

[49] L. Yan, X. Chen, Z. Wang, X. Zhang, X. Zhu, M. Zhou, W. Chen, L. Huang, V. Roy, P. Yu, G. Zhu and W. Zhang, "Size Controllable and Surface Tunable Zeolitic Imidazolate Framework-8–Poly(acrylic acid sodium salt) Nanocomposites for pH Responsive Drug Release and Enhanced in Vivo Cancer Treatment", *ACS Applied Materials & Interfaces*, vol. 9, no. 38, pp. 32990-33000, 2017.

[50]C. Adhikari, A. Das and A. Chakraborty, "Zeolitic Imidazole Framework (ZIF) Nanospheres for Easy Encapsulation and Controlled Release of an Anticancer Drug DOX under Different External Stimuli: A Way toward Smart Drug Delivery System", *Molecular Pharmaceutics*, vol. 12, no. 9, pp. 3158-3166, 2015.

[51] R. Lyndon, K. Konstas, A. Thornton, A. Seeber, B. Ladewig and M. Hill, "Visible Light-Triggered Capture and Release of CO2 from Stable Metal Organic Frameworks", *Chemistry of Materials*, vol. 27, no. 23, pp. 7882-7888, 2015.

[52] J. Jia, Y. Zhang, M. Zheng, C. Shan, H. Yan, W. Wu, X. Gao, B. Cheng, W. Liu and Y. Tang, "Functionalized Eu(III)-Based Nanoscale Metal–Organic Framework To Achieve Near-IR-Triggered and -Targeted Two-Photon Absorption Photodynamic Therapy", *Inorganic Chemistry*, vol. 57, no. 1, pp. 300-310, 2017.

[53] Z. Wang, Y. Fu, Z. Kang, X. Liu, N. Chen, Q. Wang, Y. Tu, L. Wang, S. Song, D. Ling, H. Song, X. Kong and C. Fan, "Organelle-Specific Triggered Release of Immunostimulatory Oligonucleotides from Intrinsically Coordinated DNA–Metal–

Organic Frameworks with Soluble Exoskeleton", *Journal of the American Chemical Society*, vol. 139, no. 44, pp. 15784-15791, 2017.

[54] W. Lin, Q. Hu, K. Jiang, Y. Cui, Y. Yang and G. Qian, "A porous Zn-based metal-organic framework for pH and temperature dual-responsive controlled drug release", *Microporous and Mesoporous Materials*, vol. 249, pp. 55-60, 2017.

[56] H. Yoo and T. Park, "Folate-receptor-targeted delivery of DOX nano-aggregates stabilized by DOX–PEG–folate conjugate", *Journal of Controlled Release*, vol. 100, no. 2, pp. 247-256, 2004.

[57] C. Muller and R. Schibli, "Folic Acid Conjugates for Nuclear Imaging of Folate Receptor-Positive Cancer", *Journal of Nuclear Medicine*, vol. 52, no. 1, pp. 1-4, 2010.

[58] G. Zwicke, G. Ali Mansoori and C. Jeffery, "Utilizing the folate receptor for active targeting of cancer nanotherapeutics", *Nano Reviews*, vol. 3, no. 1, p. 18496, 2012.

[59] O. Tabasi, C. Falamaki and Z. Khalaj, "Functionalized mesoporous silicon for targeted-drug-delivery", *Colloids and Surfaces B: Biointerfaces*, vol. 98, pp. 18-25, 2012.

[60] T. Thomas, B. Huang, S. Choi, J. Silpe, A. Kotlyar, A. Desai, H. Zong, J. Gam, M. Joice and J. Baker, "Polyvalent Dendrimer-Methotrexate as a Folate Receptor-Targeted Cancer Therapeutic", *Molecular Pharmaceutics*, vol. 9, no. 9, pp. 2669-2676, 2012.

[61] "X-ray Powder Diffraction (XRD)", *Techniques*, 2018. [Online]. Available: https://serc.carleton.edu/research_education/geochemsheets/techniques/XRD.html. [Accessed: 19- Apr- 2018].

[62] "X-Ray Diffraction Analysis (XRD) | Element Materials Technology", *Element.com*, 2018. [Online]. Available: https://www.element.com/materials-testing-services/x-ray-diffraction. [Accessed: 19- Apr- 2018].

[63] S. Vyazovkin, "Thermogravimetric Analysis", *Characterization of Materials*, 2012.

[64] *Perkinelmer.com*, 2018. [Online]. Available: https://www.perkinelmer.com/lab-solutions/resources/docs/faq_beginners-guide-to-thermogravimetric-analysis_009380c_01.pdf. [Accessed: 19- Apr- 2018].

[65] "FTIR Basics | Thermo Fisher Scientific", *Thermofisher.com*, 2018. [Online]. Available: http://www.thermofisher.com/in/en/home/industrial/spectroscopy-elemental-isotope-analysis/spectroscopy-elemental-isotope-analysis-learning-center/molecular-spectroscopy-information/ftir-information/ftir-basics.html. [Accessed: 19- Apr- 2018].

[66] "Scanning Electron Microscopy (SEM)", *Techniques*, 2018. [Online]. Available: https://serc.carleton.edu/research_education/geochemsheets/techniques/SEM.html. [Accessed: 19- Apr- 2018].

[67] "Dynamic Light Scattering for Nanoparticle Size Analysis - HORIBA", *Horiba.com*, 2018. [Online]. Available:

http://www.horiba.com/scientific/products/particle-characterization/technology/dynamic-light-scattering/. [Accessed: 19- Apr- 2018].

[68] A. Thakur, "Principle, working and applications of UV spectroscopy", *India Study Channel*,2020.[Online].Available: https://www.indiastudychannel.com/resources/146681-Principle-working-and-applications-of-UV-spectroscopy.aspx. [Accessed: 26- May- 2020].

[69] B. Wu, X. Lin, L. Ge, L. Wu and T. Xu, "A novel route for preparing highly proton conductive membrane materials with metal-organic frameworks", *Chem. Commun.*, vol. 49, no. 2, pp. 143-145, 2013.

[70] T. Tuan, N. Phuong and N. Ha, "Photocatalytic degradation of trinitrotoluene using material Fe-NH2-BDC (MOF)", *International Journal of Engineering Research*, vol. 6, no. 7, p. 349, 2017.

[71] N. Hoshyar, S. Gray, H. Han, and G. Bao, "The effect of nanoparticle size on in vivo pharmacokinetics and cellular interaction," *Nanomedicine*, vol. 11, no. 6, pp. 673–692, 2016.

[72] F. Perche and V. P. Torchilin, "Recent Trends in Multifunctional Liposomal Nanocarriers for Enhanced Tumor Targeting," *J. Drug Deliv.*, vol. 2013, pp. 1–32, 2013.

[73] S. Dash, P. N. Murthy, L. Nath, and P. Chowdhury, "Kinetic modeling on drug release from controlled drug delivery systems," *Acta Poloniae Pharmaceutica - Drug Research*, 2010. [Online] [Accessed 10-December-2020.

[74] G. S. Banker, J. Siepmann, and C. Rhodes, *Modern Pharmaceutics*. CRC Press,p 2002, pp. 95-127.

[75] H. Lokhandwala, A. Deshpande, and S. Deshpande, "Kinetic Modeling and Dissolution Profiles Comparission: an Overview drug release kinetic models, model dependent method, model independent method, statistical model, pairwise comparison," *Int J Pharm Bio Sci*, vol. 4, no. 1, pp. 728–737, 2013

[76] G. Singhvi and M. Singh, "International Journal of Pharmaceutical Studies and Research Review: In-Vitro Drug Release Characterization Models." *Int J Pharm Stud Res* 2. vol. 1,no. 1,pp. 77-84, 2011

[77] P. L. Chee, A. Prasad, X. Fang, C. Owh, V. J. J. Yeo, and X. J. Loh, "Supramolecular cyclodextrin pseudorotaxane hydrogels: A candidate for sustained release?," *Mater. Sci. Eng. C*, vol. 39, no. 1, pp. 6–12, Jun. 2014.

[78] M. Esperanza Adrover, M. Pedernera, M. Bonne, B. Lebeau, V. Bucalá, and L. Gallo, "Synthesis and characterization of mesoporous SBA-15 and SBA-16 as carriers to improve albendazole dissolution rate," Saudi Pharm. J., vol. 28, no. 1, pp. 15–24, Jan. 2020.

[79] A. Parmar and S. Sharma, "Engineering design and mechanistic mathematical models: Standpoint on cutting edge drug delivery," TrAC - *Trends in Analytical Chemistry*, vol. 100. pp. 15–35, 01-Mar-2018.

[80] X. Li, X. Wu, H. Yang, L. Li, Z. Ye, and Y. Rao, "A nuclear targeted Dox-aptamer loaded liposome delivery platform for the circumvention of drug resistance in breast cancer," *Biomed. Pharmacother.*, vol. 117, p. 109072, Sep. 2019.

[81] Y. Cheng et al., “DOX loaded tumor-triggered targeting ammonium bicarbonate liposomes for tumor-specific drug delivery,” *Colloids Surfaces B Biointerfaces*, vol. 178, pp. 263–268, Jun. 2019.

[82] D. Bi, L. Zhao, H. Li, Y. Guo, X. Wang, and M. Han, “A comparative study of polydopamine modified and conventional chemical synthesis method in DOX liposomes form the aspect of tumor targeted therapy,” *Int. J. Pharm.*, vol. 559, pp. 76–85, Mar. 2019.

[83] H. Zhang and P. Liu, “Bio-inspired keratin-based core-crosslinked micelles for pH and reduction dual-responsive triggered DOX delivery,” *Int. J. Biol. Macromol.*, vol. 123, pp. 1150–1156, Feb. 2019.

[84] D. Xiong, X. Zhang, S. Peng, H. Gu, and L. Zhang, “Smart pH-sensitive micelles based on redox degradable polymers as DOX/GNPs carriers for controlled drug release and CT imaging,” Colloids Surfaces B Biointerfaces, vol. 163, pp. 29–40, Mar. 2018.

[85] Y. Lu et al., “Interface crosslinked mPEG-b-PAGE-b-PCL triblock copolymer micelles with high stability for anticancer drug delivery,” Colloids Surfaces B Biointerfaces, vol. 189, p. 110830, May 2020.

[86] W. Cai, J. Wang, C. Chu, W. Chen, C. Wu and G. Liu, "Metal-Organic Framework-Based Stimuli-Responsive Systems for Drug Delivery", *Advanced Science*, vol. 6, no. 1, p. 1801526, 2018. Available: 10.1002/advs.201801526 [Accessed 22 November 2020].

[87] V. Gupta, S. Tyagi and A. Paul, "Development of Biocompatible Iron-Carboxylate Metal Organic Frameworks for pH-Responsive Drug Delivery Application", *Journal of Nanoscience and Nanotechnology*, vol. 19, no. 2, pp. 646-654, 2019.

[88] A. Cabrera-García, E. Checa-Chavarria, E. Rivero-Buceta, V. Moreno, E. Fernández, and P. Botella, “Amino modified metal-organic frameworks as pH-responsive nanoplatforms for safe delivery of camptothecin,” *J. Colloid Interface Sci.*, vol. 541, pp. 163–174, Apr. 2019.

[89] C. Lin et al., “Carbon dots embedded metal organic framework @ chitosan core-shell nanoparticles for vitro dual mode imaging and pH-responsive drug delivery,” *Microporous Mesoporous Mater.*, vol. 293, p. 109775, Feb. 2020.

Appendix A

Figure A1: Zero Order Model of the ultra-sound triggered DOX Loaded NH2-Fe BDC MOF at a pH level of 7.4 and 37 ^{o}C

Figure A2: First Order Model of the ultra-sound triggered DOX Loaded NH2-Fe BDC MOF at a pH level of 7.4 and 37 ºC

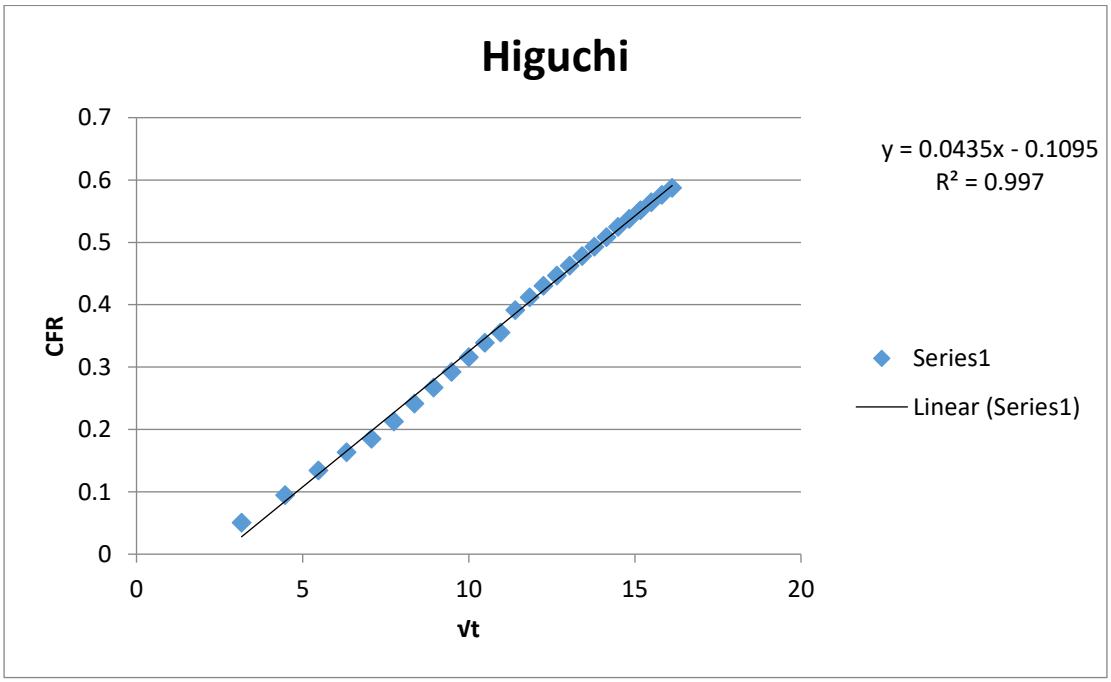

Figure A3: Higushi Model of the ultra-sound triggered DOX Loaded NH2-Fe BDC MOF at a pH level of 7.4 and 37 ºC

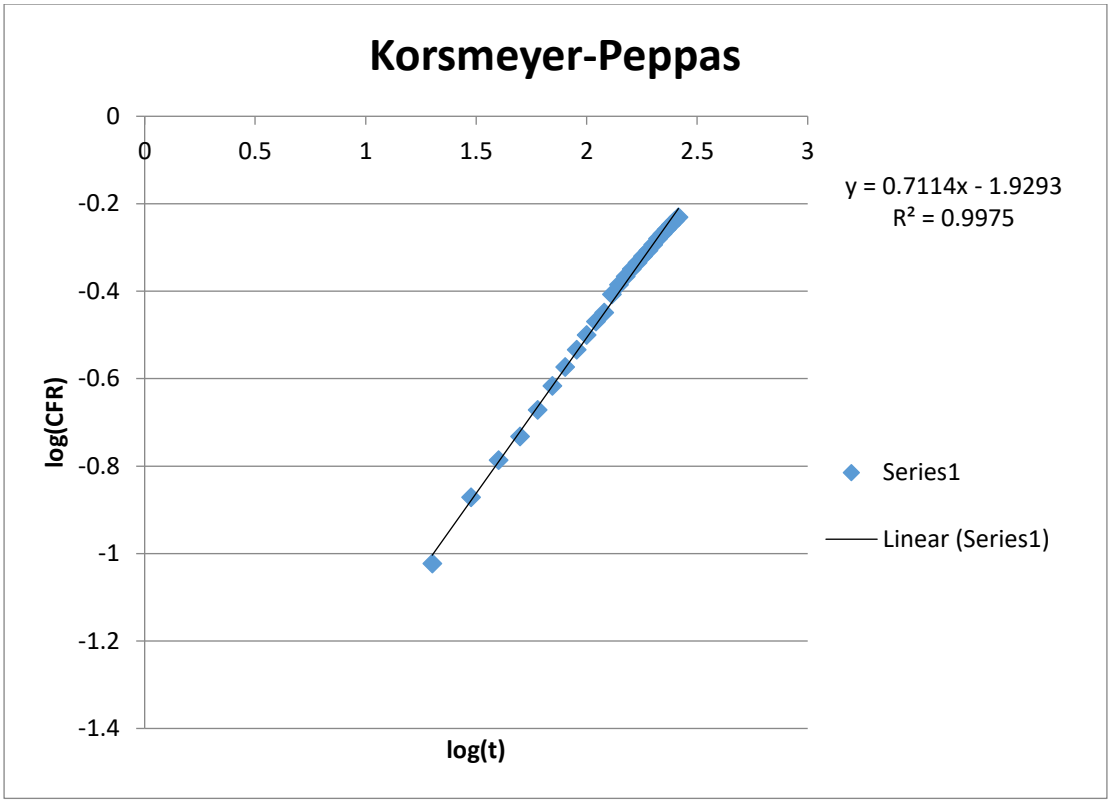

Figure A4: Korsmeyer-Peppas Model of the ultra-sound triggered DOX Loaded NH2-Fe BDC MOF at a pH level of 7.4 and 37 ºC

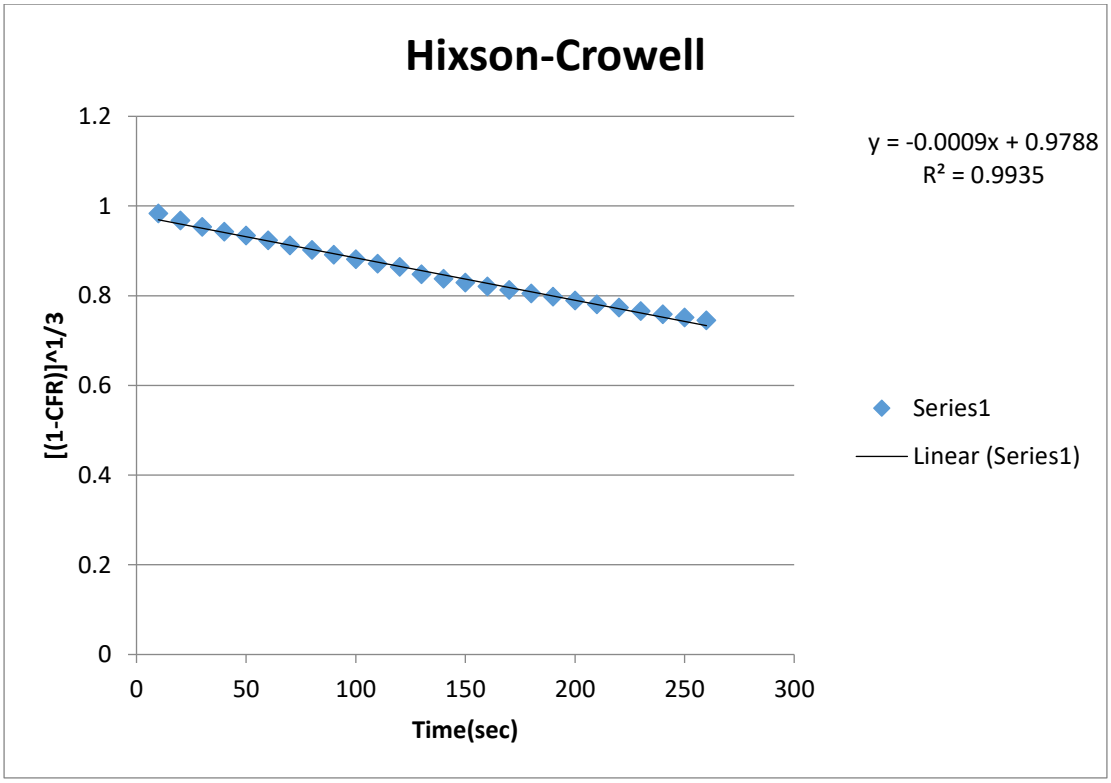

Figure A5: Hixon- Crowell Model of the ultra-sound triggered DOX Loaded NH2-Fe BDC MOF at a pH level of 7.4 and 37 ºC

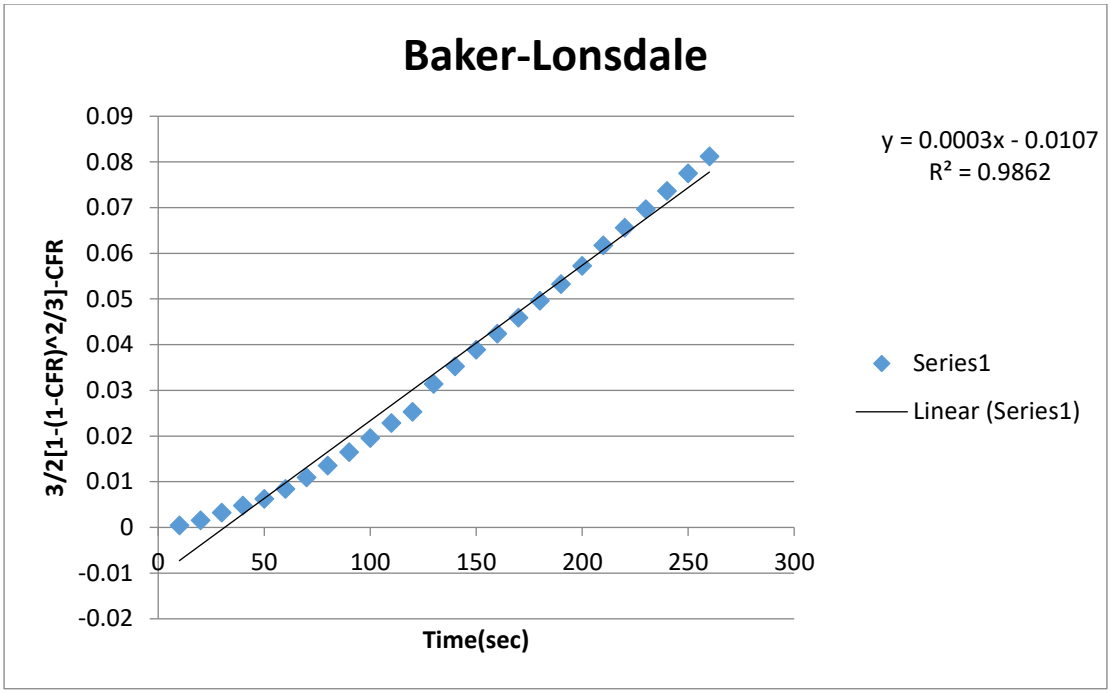

Figure A6: Baker- Lonsdale Model of the ultra-sound triggered DOX Loaded NH2-Fe BDC MOF at a pH level of 7.4 and 37 ^{o}C

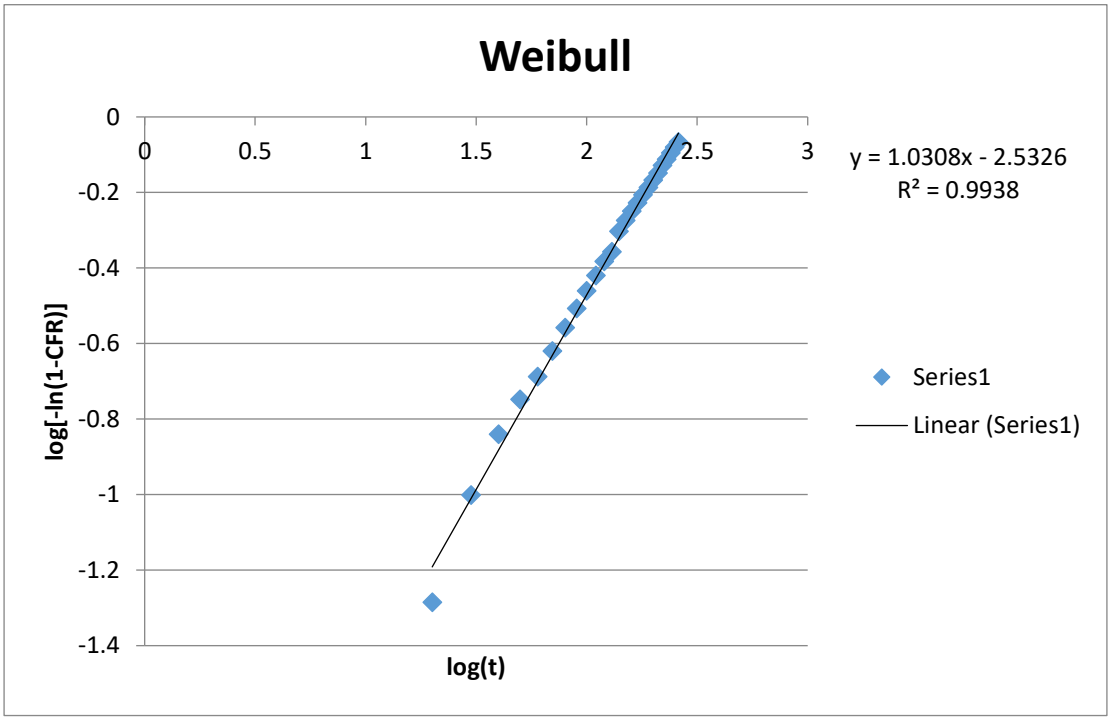

Figure A7: Weibull Model of the ultra-sound triggered DOX Loaded NH2-Fe BDC MOF at a pH level of 7.4 and 37 ^{o}C

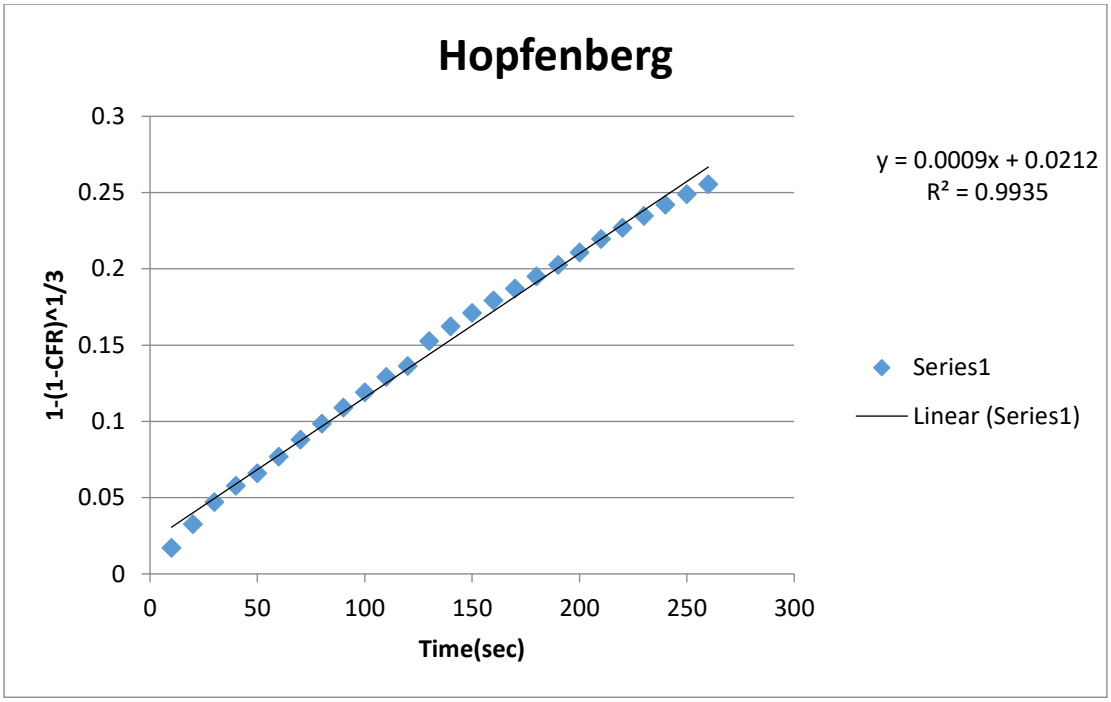

Figure A8: Hopdenberg Model of the ultra-sound triggered DOX Loaded NH2-Fe BDC MOF at a pH level of 7.4 and 37 ^{o}C

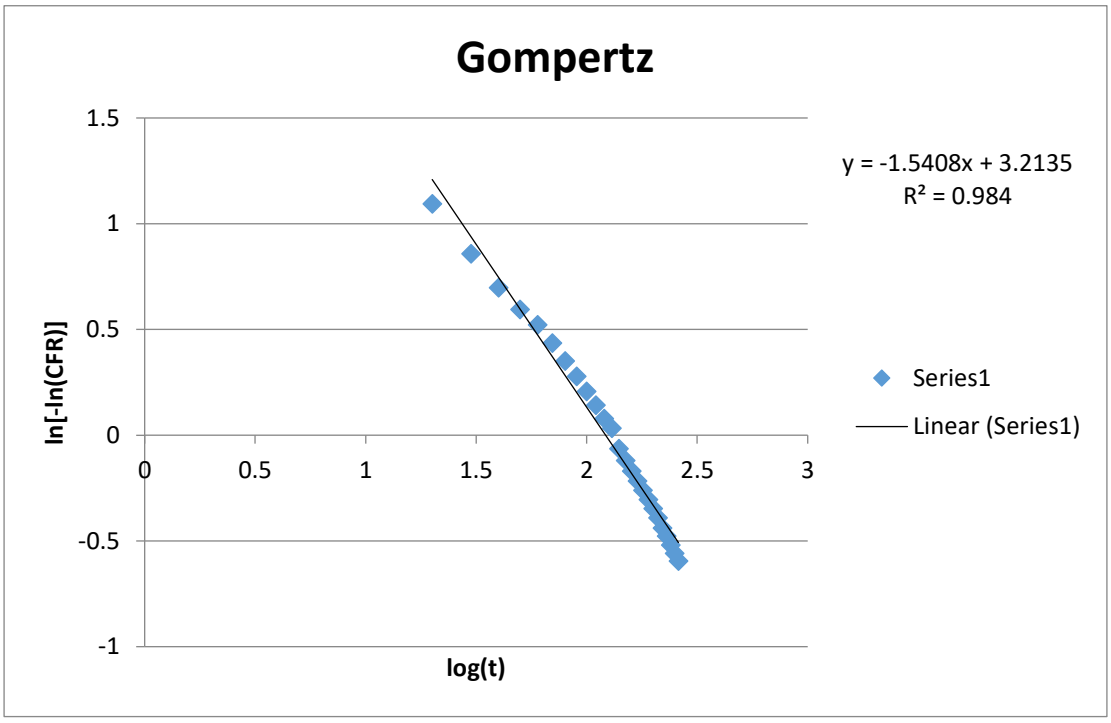

Figure A9: Gompertz Model of the ultra-sound triggered DOX Loaded NH2-Fe BDC MOF at a pH level of 7.4 and 37 ^{o}C

Figure A10: Zero Order Model of the ultra-sound triggered DOX Loaded FA-NH2-Fe BDC MOF at a pH level of 5.3 and 37 ºC

Figure A11: First Order Model of the ultra-sound triggered DOX Loaded FA-NH2-Fe BDC MOF at a pH level of 5.3 and 37 ºC

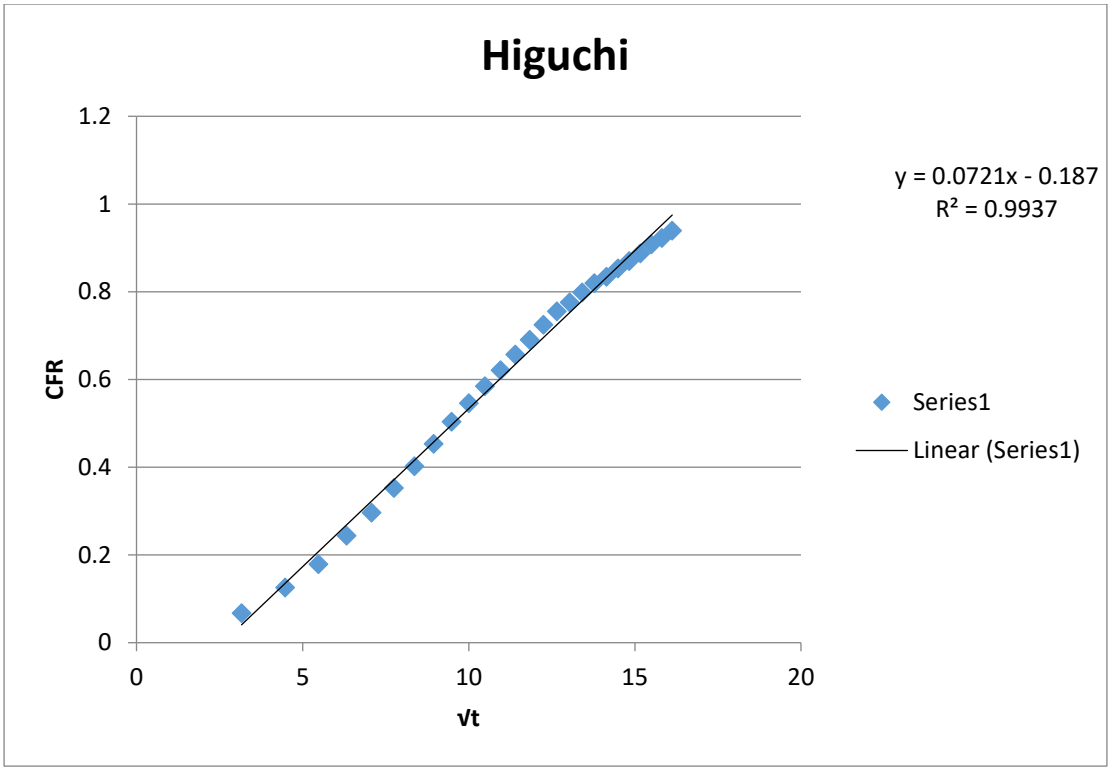

Figure A12: Higushi Model of the ultra-sound triggered DOX Loaded FA-NH2-Fe BDC MOF at a pH level of 5.3 and 37 ºC

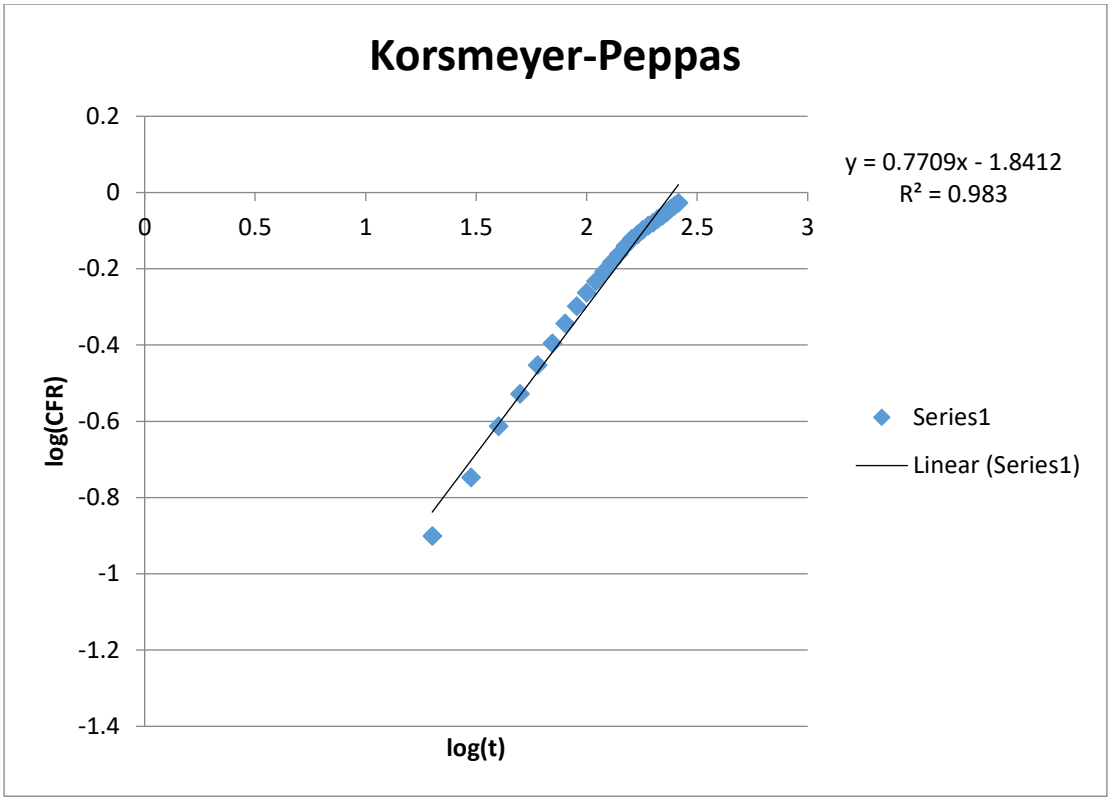

Figure A13: Korsmeyer-Peppas Model of the ultra-sound triggered DOX Loaded FA-NH2-Fe BDC MOF at a pH level of 5.3 and 37 ^{o}C

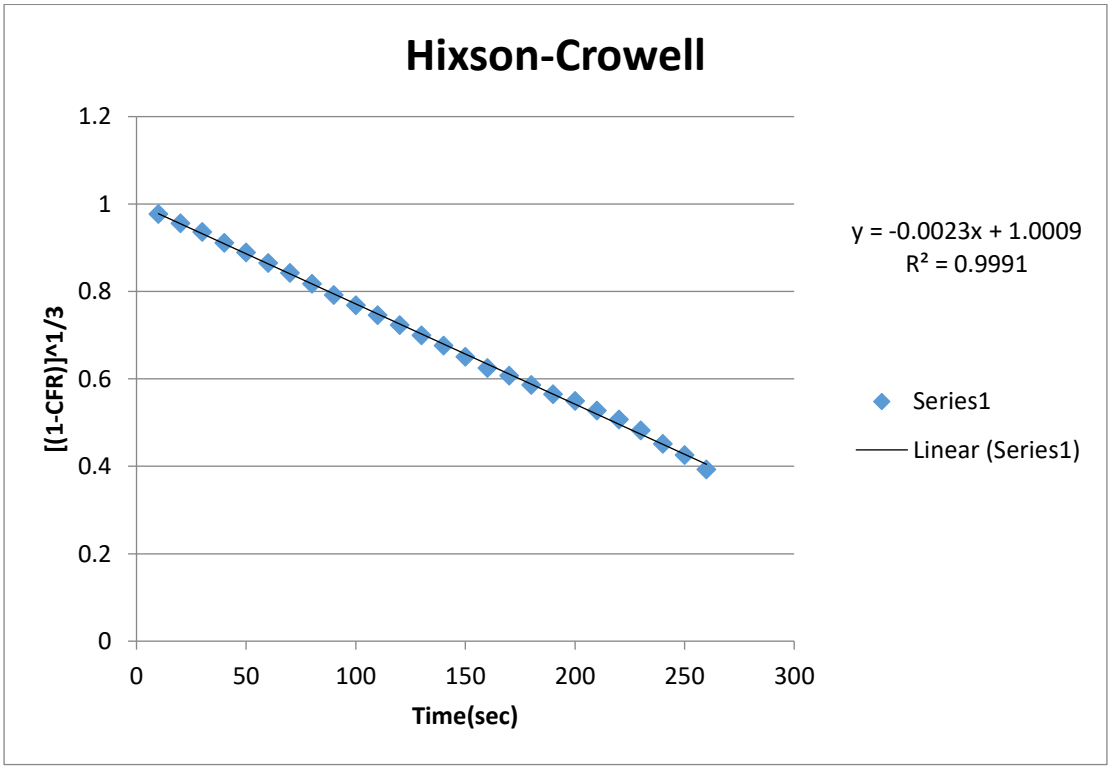

Figure A14: Hixon- Crowell Model of the ultra-sound triggered DOX Loaded FA-NH2-Fe BDC MOF at a pH level of 5.3 and 37 ^{o}C

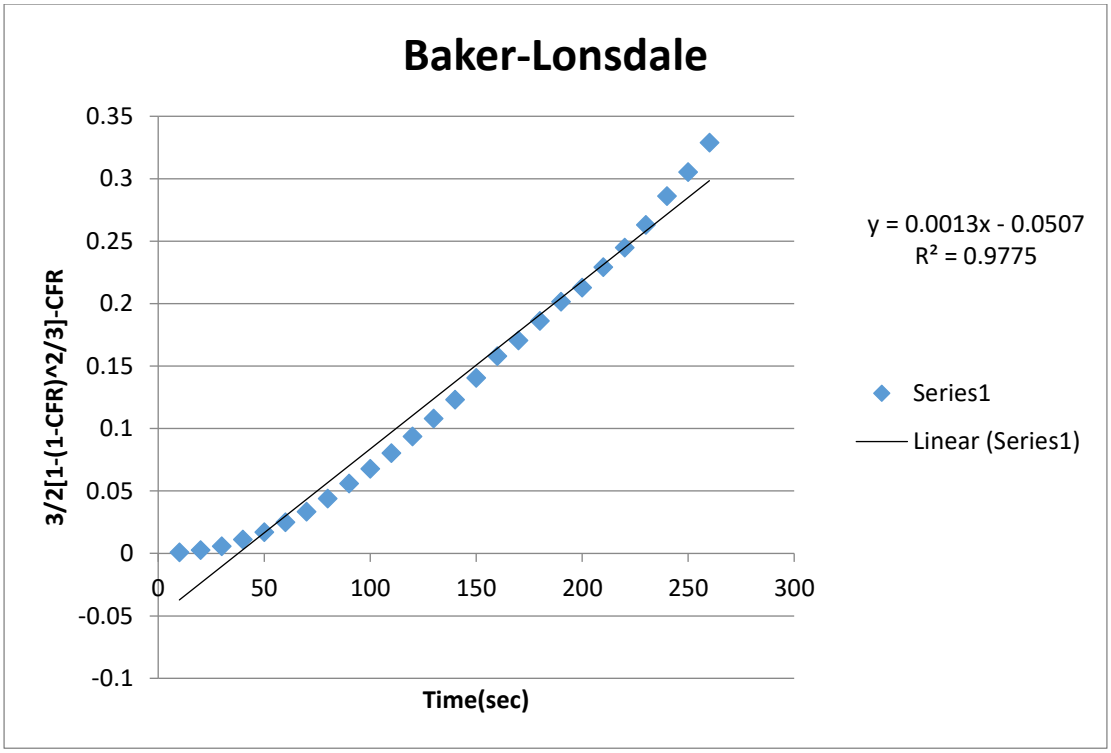

Figure A15: Baker- Lonsdale Model of the ultra-sound triggered DOX Loaded FA-NH2-Fe BDC MOF at a pH level of 5.3 and 37 ºC

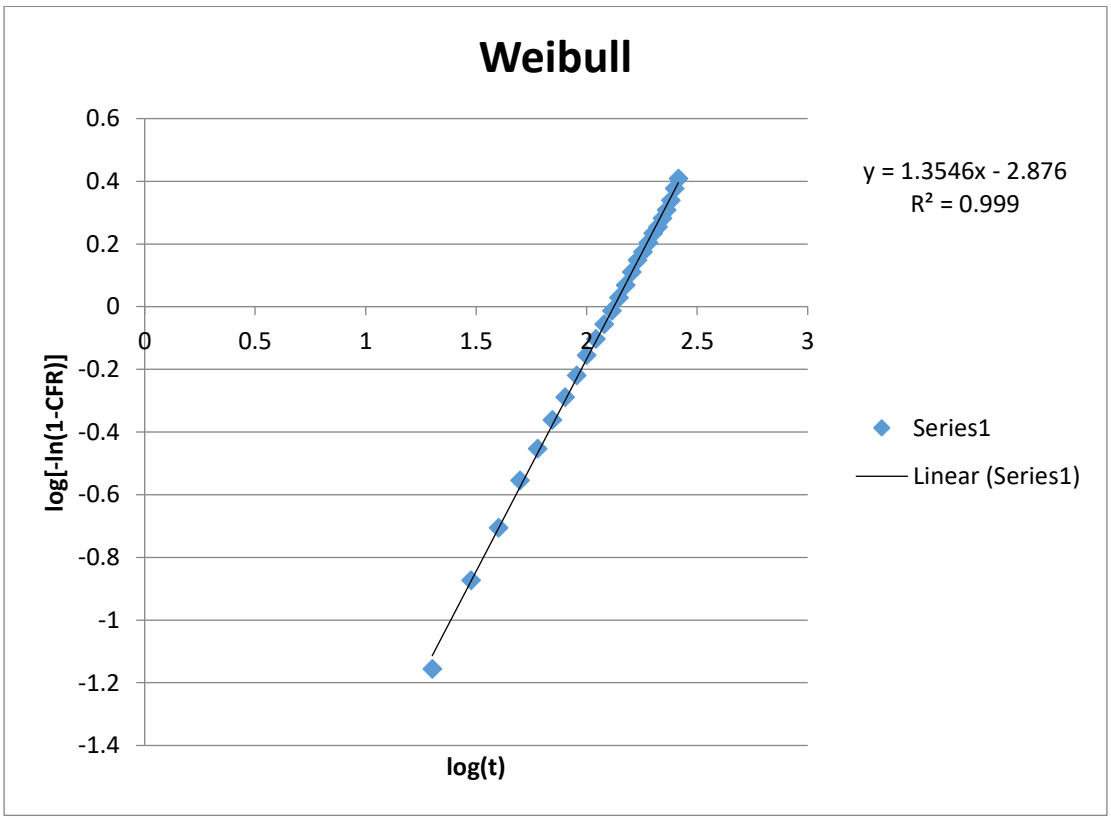

Figure A16: Weibull Model of the ultra-sound triggered DOX Loaded FA-NH2-Fe BDC MOF at a pH level of 5.3 and 37 ºC

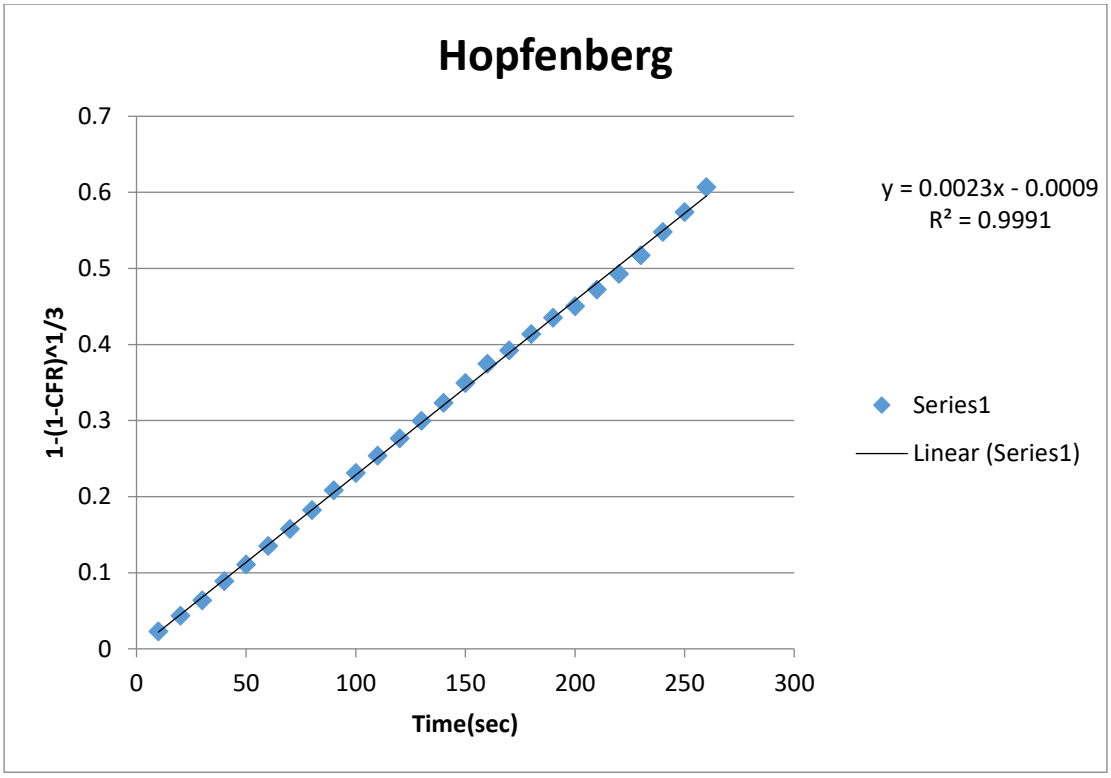

Figure A17: Hopdenberg Model of the ultra-sound triggered DOX Loaded FA-NH2-Fe BDC MOF at a pH level of 5.3 and 37 ^{o}C

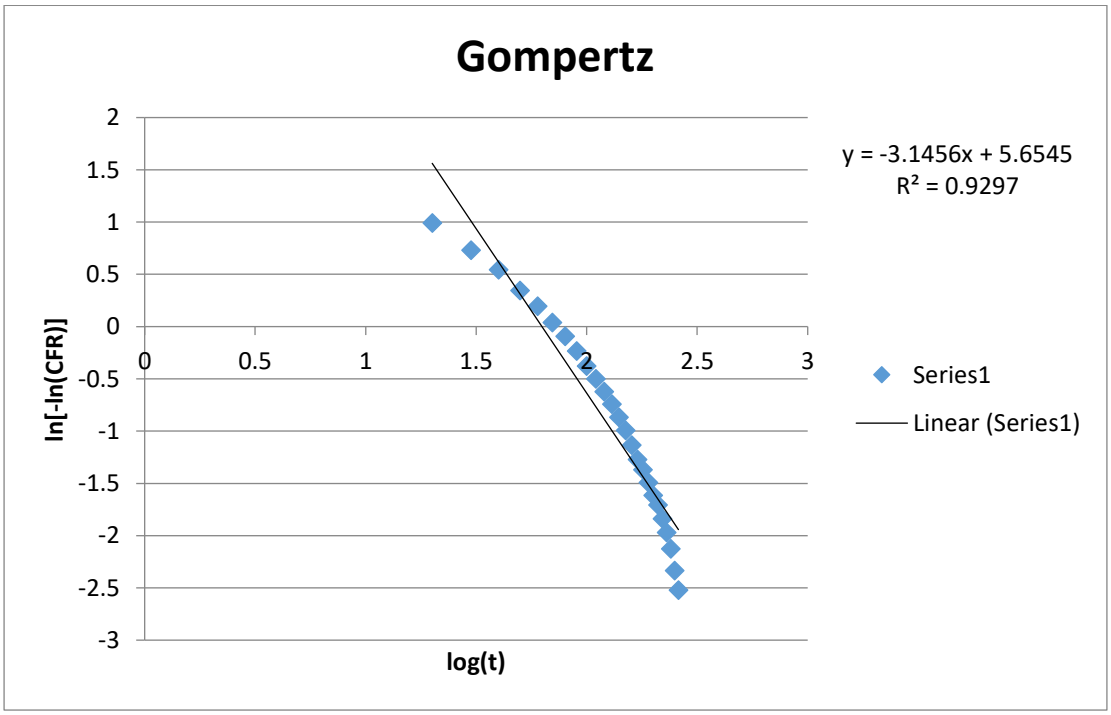

Figure A18:Gompertz Model of the ultra-sound triggered DOX Loaded FA-NH2-Fe BDC MOF at a pH level of 5.3 and 37 ^{o}C

Figure A19: Zero Order Model of the ultra-sound triggered DOX Loaded NH2-Fe BDC MOF at a pH level of 5.3 and 37 ºC

Figure A20:First Order Model of the ultra-sound triggered DOX Loaded NH2-Fe BDC MOF at a pH level of 5.3 and 37 ºC

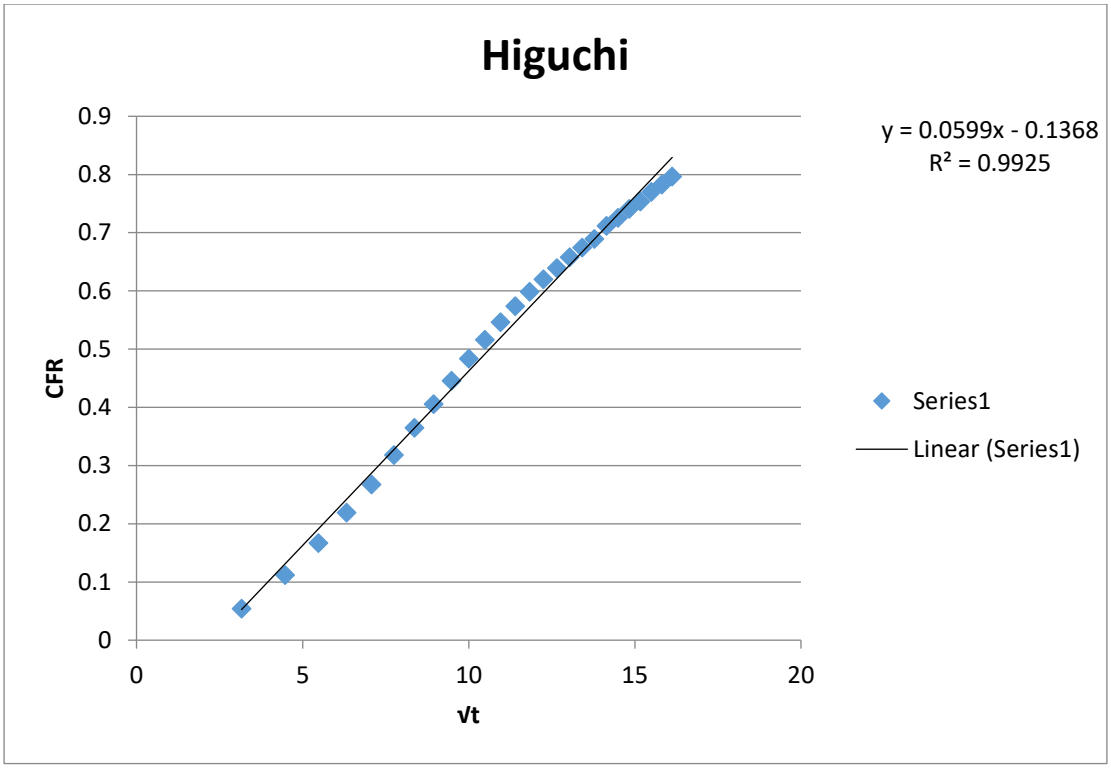

Figure A21: Higushi Model of the ultra-sound triggered DOX Loaded NH2-Fe BDC MOF at a pH level of 5.3 and 37 °C

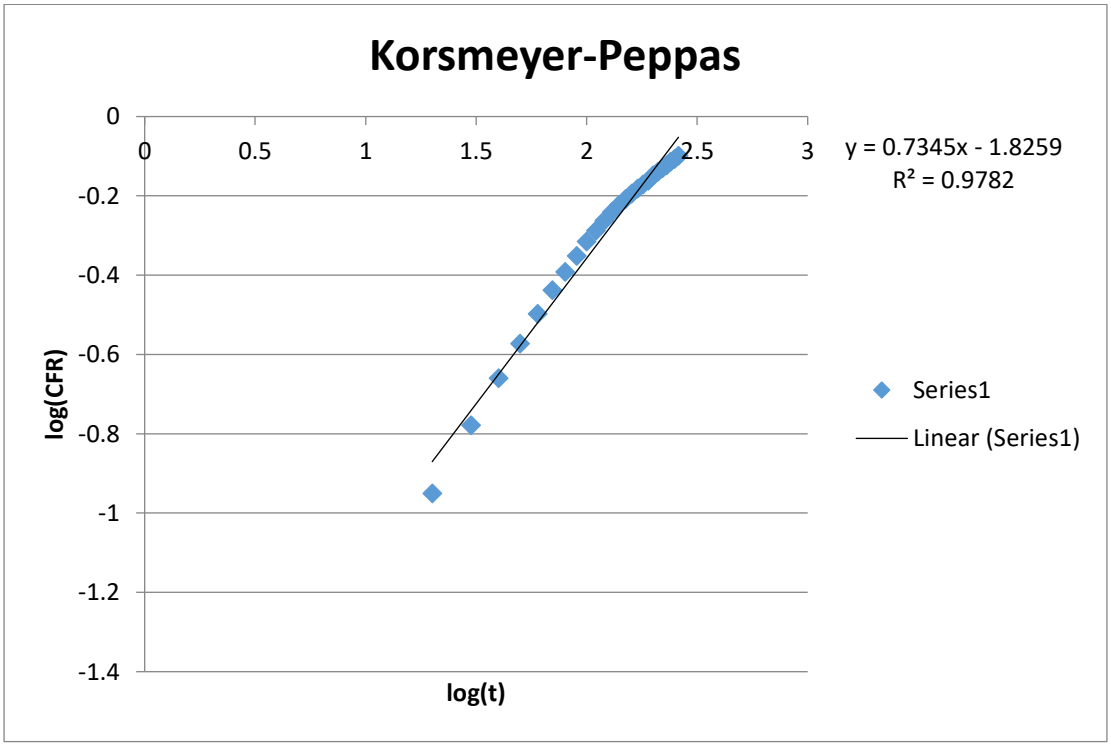

Figure A22: Korsmeyer-Peppas Model of the ultra-sound triggered DOX Loaded NH2-Fe BDC MOF at a pH level of 5.3 and 37 °C

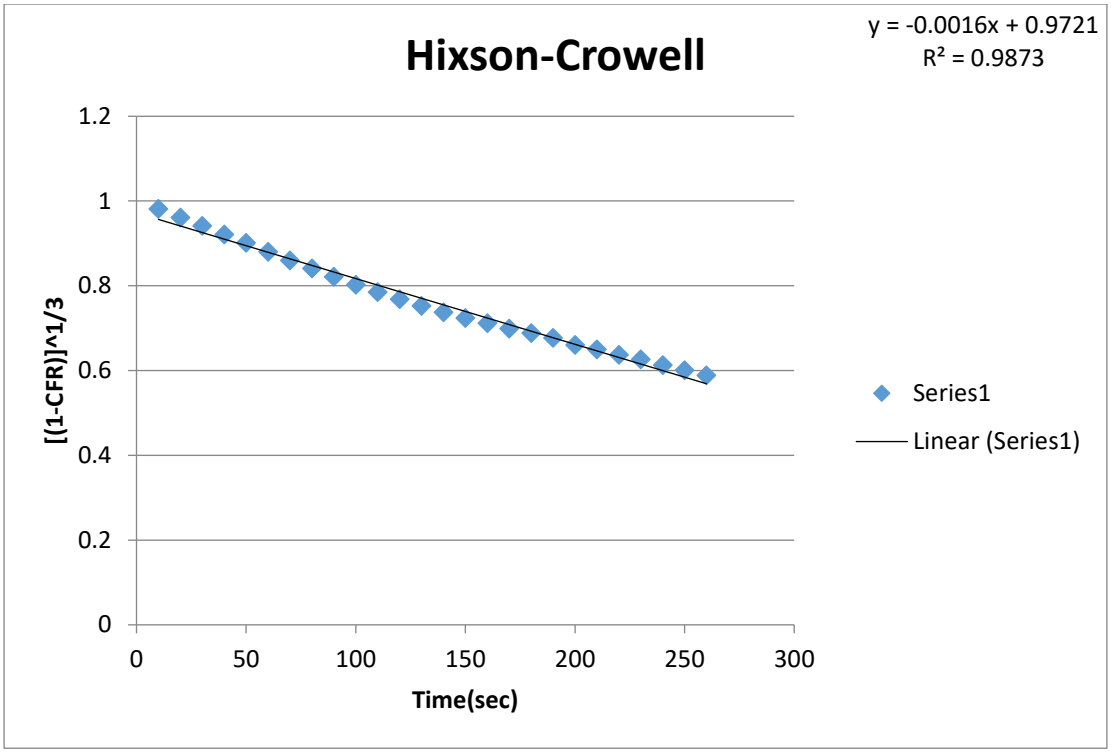

Figure A23: Hixon- Crowell Model of the ultra-sound triggered DOX Loaded NH2-Fe BDC MOF at a pH level of 5.3 and 37 ^{o}C

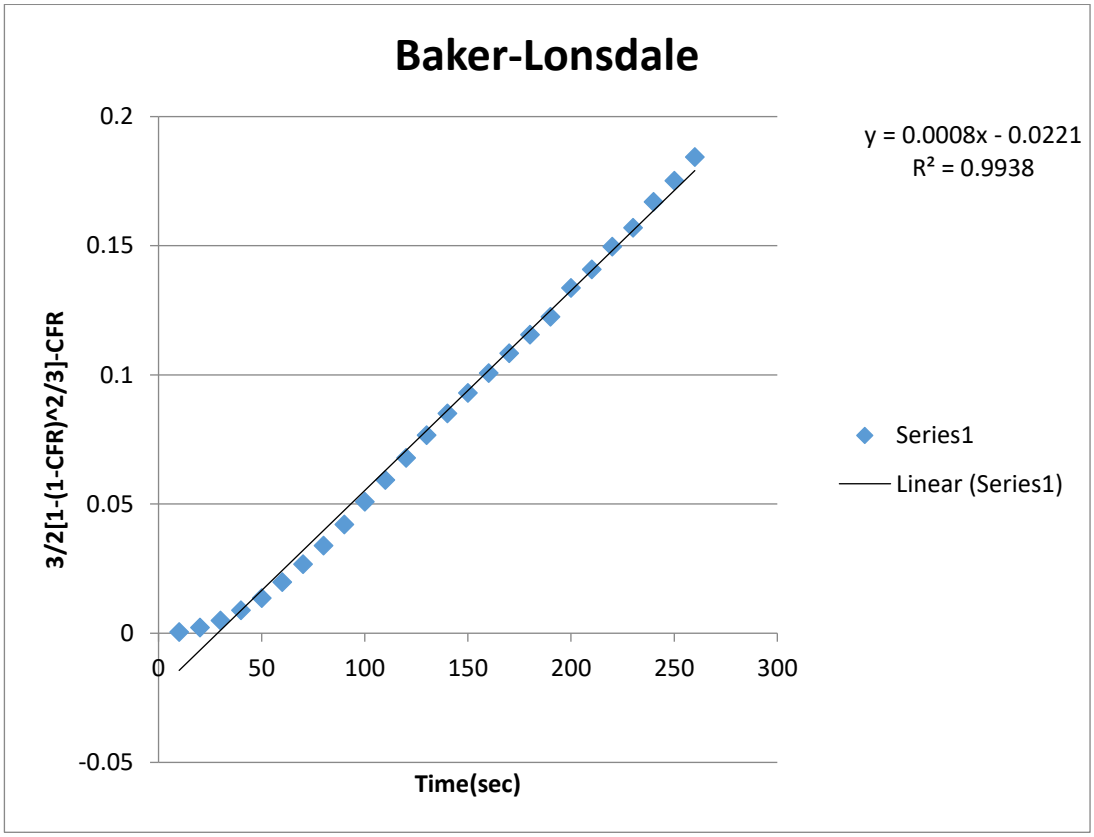

Figure A24: Baker- Lonsdale Model of the ultra-sound triggered DOX Loaded NH2-Fe BDC MOF at a pH level of 5.3 and 37 ^{o}C

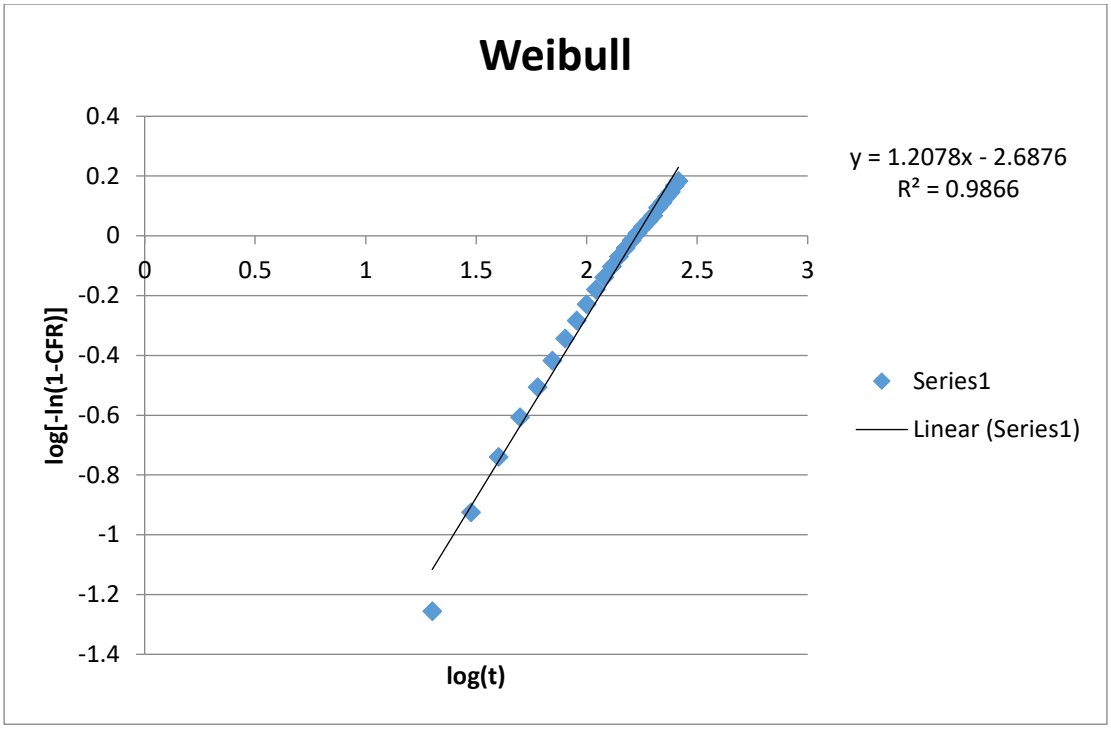

Figure A25: Weibull Model of the ultra-sound triggered DOX Loaded NH2-Fe BDC MOF at a pH level of 5.3 and 37 ^{o}C

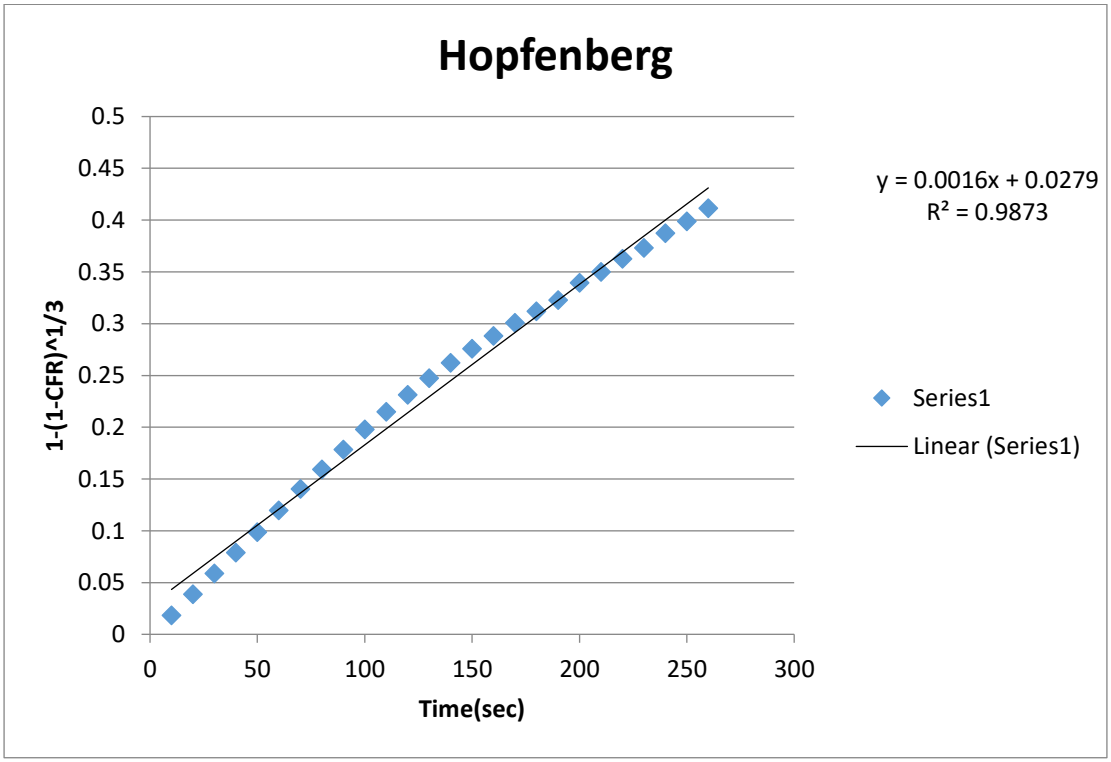

Figure A26: Hopdenberg Model of the ultra-sound triggered DOX Loaded FA-NH2-Fe BDC MOF at a pH level of 5.3 and 37 ^{o}C

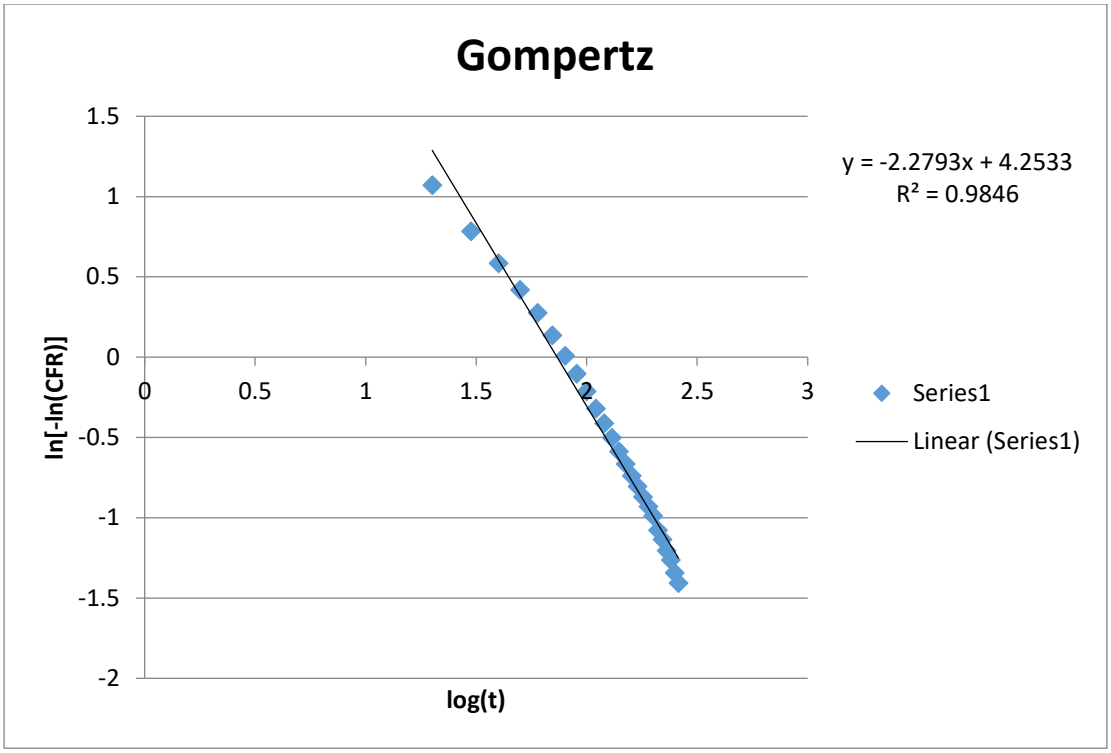

Figure A27: Gompertz Model of the ultra-sound triggered DOX Loaded NH2-Fe BDC MOF at a pH level of 5.3 and 37 ^{o}C

Vita

Ahmed H.S Ahmed was born in the city of Amman, Jordan and was raised in Ramallah, Palestine. Mr. Ahmed was educated at Al-Mustaqbal private school where he finished his High school degree and A- level Cambridge examinations in 2012. Mr. Ahmed attended the American University of Sharjah, Sharjah, UAE and received a bachelor's of science in Chemical Engineering in 2017. In 2017 Mr. Ahmed began his master's program in Chemical Engineering at the American University of Sharjah.